



**Synthesis, molecular structure and electrochemical properties of nickel(II) benzhydrazone complexes: Influence of ligand Substitution on DNA/Protein interaction, antioxidant and cytotoxicity**

Journal:	<i>RSC Advances</i>
Manuscript ID	RA-ART-09-2015-019530.R1
Article Type:	Paper
Date Submitted by the Author:	06-Nov-2015
Complete List of Authors:	Ramasamy, Raj; Bharathidasan University, School of Chemistry Rengan, Ramesh; Bharathidasan University, School of Chemistry;
Subject area & keyword:	Bioinorganic chemistry < Chemical biology & medicinal



## Synthesis, molecular structure and electrochemical properties of nickel(II) benzhydrazone complexes: Influence of ligand Substitution on DNA/Protein interaction, antioxidant and cytotoxicity†

Received 00th January 20xx,  
Accepted 00th January 20xx

DOI: 10.1039/x0xx00000x

www.rsc.org/

Ramasamy Raj Kumar and Rengan Ramesh\*

A series of new nickel(II) benzhydrazone complexes having general formula  $[\text{Ni}(\text{L})_2]$  (where L=thiophene aldehyde benzhydrazone) have been synthesized from the reaction of  $\text{Ni}(\text{OAc})_2 \cdot 4\text{H}_2\text{O}$  with 2 equivalent of benzhydrazone ligands in DMF/ethanol medium. The complexes have been characterized by analytical, spectral (FT-IR, UV-Vis, NMR and ESI-Mass) and single crystal X-ray crystallography methods. All the complexes exhibit quasi-reversible one electron reduction responses ( $\text{Ni}^{\text{II}}/\text{Ni}^{\text{I}}$ ) within the  $E_{1/2}$  range -0.71 to -0.77 V versus SCE. The structure of one of the complexes has been determined by single crystal X-ray diffraction study shows that coordination of benzhydrazone ligands to the nickel via azomethine nitrogen and imidolate oxygen atom as a monobasic bidentate donor provided by two units of the ligand with square planar geometry. The DNA binding interactions of the complexes with calf thymus DNA have been investigated by absorption, emission, electrochemical, circular dichromism and viscosity measurements revealed that the complexes could interact with DNA through intercalation. The protein binding interactions of the complexes with BSA was investigated by UV-Vis, fluorescence and synchronous fluorescence methods which indicated the stronger binding nature of the complexes with BSA and a static quenching mechanism was observed. Further the free radical scavenging potential of all the complexes were also carried out against DPPH radical, hydroxyl radical and nitric oxide radical under in vitro conditions. Furthermore, the cytotoxicity of all the complexes examined in vitro on a human cervical cancer cell line HeLa, MCF-7 and a normal mouse embryonic fibroblasts cell line NIH-3T3 under identical conditions and exhibited good  $\text{IC}_{50}$  value. These values were further supported by neutral red uptake assay of HeLa cell lines. The AO-EB/DAPI staining assays and flow cytometry analysis revealed that the complexes induce cell death only through apoptosis.

### Introduction

The interaction of metal complexes with DNA has long been the subject of great interest in relation to the development of new reagents for biotechnology and medicine.<sup>1-3</sup> A number of biological experiments have also reveal that DNA is the main intracellular target of anticancer drugs due to the interaction between small molecules and DNA, which can cause DNA damage in cancer cells, hold up the division of cancer cells and resulting in cell death.<sup>4</sup> The accidental discovery of the anti-

tumoral properties of cisplatin by Rosenberg and co-workers<sup>5</sup> was followed one of the most impressive drug success stories ever and significant improvement of cancer therapy. Besides cisplatin several platinum complexes (carboplatin, oxaliplatin, nedaplatin and lobaplatin) have been approved for current tumour therapy. Complexes of ruthenium, titanium, or gallium have already been tested in clinical phase I and phase II studies.<sup>7, 8</sup> Preclinical research involves also metal complexes containing other non platinum metals (e.g. iron, cobalt, gold).<sup>9</sup>

The interactions of metal complexes with serum albumins have received enough attention in the scientific community by studying the antitumoral metallopharmaceutical pharmacodynamics and structure-activity relationships.<sup>10</sup> Serum albumins are the most abundant proteins in plasma that have many physiological functions.<sup>11-13</sup> Particularly, they contribute to control osmotic blood pressure and maintenance of blood pH.<sup>14</sup> BSA is the most well studied serum albumins, due to its structural resemblance with human serum albumin (HSA).

\*School of Chemistry Bharathidasan University,  
Tiruchirappalli – 620 024, Tamil Nadu, India.

Corresponding author:

E-mail: ramesh\_bdu@yahoo.com; rrameshbdu@gmail.com

Fax: +0091-431-2407045/2407020; Tel: +91-431-2407053

†Electronic Supplementary Information (ESI) available:

[The UV-Vis, ESI-Mass and Cyclic Voltammograms of the complexes]

CCDC reference number 1032855.

See DOI: 10.1039/b000000x/

Free radicals inside the human body play a pathogenic role in most of the chronic degenerative diseases while include inflammatory, cancer, autoimmune, cardiovascular and neurodegenerative diseases and aging.<sup>15-18</sup> Free radicals can adversely affect lipids, proteins and DNA and have been implicated in the aging process and in a number of human diseases. Antioxidants are capable of neutralising these reactive species in terms of prevention, interception and damage repair.<sup>19,20</sup>

Hydrazones are important class of ligands with interesting ligation properties due to the existence of several coordination sites<sup>21</sup> and are broadly applies in the field of medicines, insecticides and analytical reagents due to their superior bioactivity.<sup>22</sup> The hydrazone unit offers a number of interesting features like the degree of rigidity, a conjugated  $\pi$  system and a NH unit that readily participates in hydrogen bonding and may be a site of protonation-deprotonation. Some hydrazone analogs have been explored as potential oral iron chelating drugs for the remedy of genetic disorders such as thalassemia and have also been advised as possible metal chelating agents for treating neurodegenerative disorders such as Alzheimer disease.<sup>23-25</sup> Hydrazone ligands create an environment similar to the one present in biological systems usually by making coordination through oxygen and nitrogen atoms. In this esteem, the formation of metal complexes plays a substantial role to enhance their biological activity.

Although not accepted until the 1970s, nickel plays important roles as a catalytic center in both redox and nonredox enzymes, where it has important consequences in human health (e.g., urease), energy science (e.g., hydrogenase), and the environment (e.g., carbon monoxide dehydrogenases).<sup>26</sup> Nickel(II) compounds which can be reversibly reduced to nickel(I) species have been attracting attention as models of redox active nickel containing enzymes<sup>27</sup> and as electrocatalysts.<sup>28</sup> Complementing its natural biochemical functions, complexes of nickel too display pharmacological potential. Nickel(II) complexes are regarded as one of the most promising alternatives to the traditional cisplatin as anticancer drugs; an idea supported by an extensive number of research articles describing the synthesis, DNA-binding and cytotoxic activities of numerous nickel(II) complexes.<sup>29-31</sup> The synthesis, structure, DNA-binding properties and antioxidant activity of a nickel(II) complex with bis(*N*-allylbenzimidazol-2-ylmethyl) benzylamine has been reported.<sup>32</sup> Synthesis, characterisation and in vitro pharmacological evaluation of new water soluble Ni(II) complexes of 4*N* substituted thiosemicarbazones of 2-oxo-1,2-dihydroquinoline-3-carboxaldehyde have been described.<sup>33</sup> Synthesis, structure and biological activity of nickel(II) complexes with mefenamato and nitrogen-donor ligands has been reported.<sup>34</sup> Variation in the biomolecular interactions of nickel(II) hydrazone complexes upon tuning the hydrazide fragment have been reported.<sup>35</sup>

Therefore, considerable attempts are being made to research the interaction of nickel(II) complexes with DNA and their cytotoxic activities. Based on the above facts and considering role and activity of nickel and its complexes in

biological systems, along with the significance of hydrazones in medicine, we report in this work a systematic study on synthesis, structure and electrochemical properties of nickel(II) complexes containing thiophene aldehyde benzhydrazone ligands and their interaction with DNA/protein, antioxidant and cytotoxicity. In addition, the substituent effect of nickel(II) complexes on the above said properties also studied in detail.

## Experimental Section

### Materials and Instrumentation

Nickel(II) acetate tetrahydrate, thiophene-2-carboxaldehyde and benzhydrazone derivatives were purchased from Merck and Aldrich chemicals and were used as received. Solvents were dried and freshly distilled prior to use. Calf-thymus DNA (CT-DNA) and ethidium bromide (EtBr) purchased from Sigma-Aldrich chemie were used as received. Bovine serum albumin (BSA) was purchased from Himedia Company. 3-(4, 5-Dimethylthiazol-2-yl)-2, 5-diphenyltetrazolium bromide (MTT) were purchased from Sigma-Aldrich and used as received. Human cervical cancer cells and MCF-7 human breast cancer cells were obtained from National centre for cell Science (NCCS), Pune, India. Annexin V-FITC Kit (APOAF-20TST) from sigma Aldrich was utilized as per the instruction from the manufacturer. All other chemicals and reagents used for the biological studies were of high quality in biological grade. Elemental analyses were performed on a vario EL III CHNS elemental analyser. Melting points were performed with an electrical instrument and are uncorrected. Infrared spectra were recorded in KBr pellets with a JASCO 200 plus spectrometer. The NMR spectra were recorded in DMSO- $d_6$  for the ligands and complexes with a Bruker 400 MHz instrument using TMS as the internal reference. Mass spectrometric analysis was performed by using the ESI technique on a waters Q TOF micro mass spectrometer for all these complexes upon dissolving in DMF. Electronic spectroscopy was recorded with a Cary 300 Bio Varian spectrophotometer using cuvettes of 1 cm path length. Emission intensity measurements were carried out using a Jasco FP-6500 spectrofluorimeter. The circular dichromism spectra were recorded using a JASCO J-810 spectropolarimeter equipped with a peltier Temperature control device at room temperature with a quartz cell of 1cm path length. Each sample solution was the average of 3 accumulations using a scan speed of 500 nm/ min at 1s response time. The viscosity measurements were carried out on a Schott Gerate AVS 310 viscometer at  $29 \pm 0.1^\circ\text{C}$  in a thermostatic waterbath. The supporting electrolyte tetrabutyl ammonium perchlorate (TBAP) was purchased from Aldrich and dried in vacuum prior to use. Electrochemical measurements were made using CH instruments using a glassy carbon-working electrode and 0.05 M  $[(n-C_4H_9)_4N] (ClO_4)$  (TBAP) as supporting electrolyte. All the potentials were referenced to saturated calomel electrode (SCE) and the solutions were purged with  $N_2$  before each set of experiments.

### Preparation of benzhydrazone ligands

The mono basic bidentate benzhydrazone ligands were prepared by reported procedure.<sup>36</sup> To a stirred ethanolic solution (10 mL) of 4-substituted benzhydrazide (68-85 mg, 5 mmol), an ethanolic (10 mL) solution of thiophene-2-aldehyde (0.46 mL, 56-63 mg, 5 mmol) was added dropwise. The reaction mixture was refluxed for 3 h, the solution concentrated to 5 mL and cooled to room temperature. The solid formed was filtered, washed with cold methanol (5 mL) and dried in air.

**Benzoic acid thiophene-2-ylmethylene-hydrazide. (HL1):** Colour: Cream; Yield: 87%; M.p.: 150°C; Ana. Cal. For  $C_{12}H_{10}N_2OS$  (230.29 g mol<sup>-1</sup>): C, 62.58; H, 4.37; N, 12.16; S, 13.92. Found: C, 62.53; H, 4.40; N, 12.10; S, 13.96. IR (KBr, cm<sup>-1</sup>): 3254 s  $\nu_{(N-H)}$ , 1644 s  $\nu_{(C=N)} + \nu_{(C=O)}$ . <sup>1</sup>H NMR (400 MHz, DMSO-d<sub>6</sub>)  $\delta$  (ppm): 11.8(s, 1H, NH), 8.7(s, 1H, CH=N), 7.2-8.0 (m, 8H, aromatic). UV-Vis (DMF): 265, 322 nm.

**4-chloro-benzoic acid thiophene-2-ylmethylene-hydrazide. (HL2):** Colour: Cream; Yield: 86%; M.p.: 156°C; Ana. Cal. For  $C_{12}H_9ClN_2OS$  (264.73 g mol<sup>-1</sup>): C, 54.44; H, 3.42; N, 10.58; S, 12.11. Found: C, 54.48; H, 3.46; N, 10.60; S, 12.14. IR (KBr, cm<sup>-1</sup>): 3280 s  $\nu_{(N-H)}$ , 1639 s  $\nu_{(C=N)} + \nu_{(C=O)}$ . <sup>1</sup>H NMR (400 MHz, DMSO-d<sub>6</sub>)  $\delta$  (ppm): 11.9(s, 1H, NH), 8.7(s, 1H, CH=N), 7.2-8.0 (m, 7H, aromatic). UV-Vis (DMF): 268, 324 nm.

**4-Bromo-benzoic acid thiophene-2-ylmethylene-hydrazide. (HL3):** Colour: Cream; Yield: 84%; M.p.: 158°C; Ana. Cal. For  $C_{12}H_9BrN_2OS$  (309.18 g mol<sup>-1</sup>): C, 46.61; H, 2.93; N, 9.06; S, 10.37. Found: C, 46.60; H, 2.98; N, 9.05; S, 10.25. IR (KBr, cm<sup>-1</sup>): 3296 s  $\nu_{(N-H)}$ , 1636 s  $\nu_{(C=N)} + \nu_{(C=O)}$ . <sup>1</sup>H NMR (400 MHz, DMSO-d<sub>6</sub>)  $\delta$  (ppm): 11.9(s, 1H, NH), 8.7(s, 1H, CH=N), 7.1-7.9 (m, 7H, aromatic). UV-Vis (DMF): 268, 323 nm.

**4-methoxy-benzoic acid thiophene-2-ylmethylene-hydrazide. (HL4):** Colour: Cream; Yield: 87%; M.p.: 162°C; Ana. Cal. For  $C_{13}H_{12}N_2O_2S$  (260.31 g mol<sup>-1</sup>): C, 59.98; H, 4.64; N, 10.76; S, 12.31. Found: C, 60.01; H, 4.63; N, 12.34; S, 12.29. IR (KBr, cm<sup>-1</sup>): 3272 s  $\nu_{(N-H)}$ , 1642 s  $\nu_{(C=N)} + \nu_{(C=O)}$ . <sup>1</sup>H NMR (400 MHz, DMSO-d<sub>6</sub>)  $\delta$  (ppm): 11.7(s, 1H, NH), 8.7(s, 1H, CH=N), 7.2-8.9 (m, 7H, aromatic), 3.8(s, 3H, OCH<sub>3</sub>). UV-Vis (DMF): 268, 324 nm.

### Synthesis of new square planar nickel(II) benzhydrazone complexes

All the reactions were carried out under anhydrous conditions and the new nickel(II) complexes were prepared according to the following procedure.<sup>37</sup> A hot solution Ni (CH<sub>3</sub>COO)<sub>2</sub>·4H<sub>2</sub>O (1 mmol) in ethanol was added to boiling solution of the benzhydrazone ligands (2 mmol) (HL1-HL4) in DMF. The reaction mixtures were heated to reflux for 5 h. An orange colored mononuclear complex [Ni(L)<sub>2</sub>] precipitated. The solid was separated by filtration and washed with ethanol and diethyl ether then dried under vacuum.

#### [Ni (L1)<sub>2</sub>] (1)

Color: Orange; Yield: 91.9%; M.P.: 328°C; Ana. Cal. For  $C_{24}H_{18}N_4S_2O_2Ni$  (517.25 g mol<sup>-1</sup>): C, 55.72; H, 3.50; N, 10.83; S, 12.39. Found: C, 55.80; H, 3.59; N, 10.88; S, 12.38. IR (KBr, cm<sup>-1</sup>): 1526 s  $\nu_{(C=N-N=C)}$ , 1242 s  $\nu_{(C-O)}$ . UV-Vis in DMF:  $\lambda_{max}/nm$  ( $\epsilon_{max}/dm^3mol^{-1}cm^{-1}$ ) 268(60,470) (intra-ligand transition),

361(10326) (LMCT), 424 (1965) (forbidden d→d transition). ESI-MS: m/z 522.85

#### [Ni (L2)<sub>2</sub>] (2)

Color: Orange. Yield: 89%. M.P. 340°C; Anal. Calc. for  $C_{24}H_{16}Cl_2N_4S_2O_2Ni$  (586.14 g mol<sup>-1</sup>): C, 49.17; H, 2.75; N, 9.55; S, 10.94. Found: C, 49.22; H, 2.68; N, 9.50; S, 10.98. IR (KBr, cm<sup>-1</sup>): 1583 s  $\nu_{(C=N-N=C)}$ , 1238 s  $\nu_{(C-O)}$ . UV-Vis in DMF:  $\lambda_{max}/nm$  ( $\epsilon_{max}/dm^3mol^{-1}cm^{-1}$ ) 266(86,760) (intra-ligand transition), 363(14308) (LMCT), 424 (1086) (forbidden d→d transition). ESI-MS: m/z 592.57

#### [Ni (L3)<sub>2</sub>] (3)

Color: Orange. Yield: 88.49%. M.P. 344°C; Anal. Calc. for  $C_{24}H_{16}Br_2N_4S_2O_2Ni$  (675.05 g mol<sup>-1</sup>): C, 42.70; H, 2.38; N, 8.29; S, 9.50. Found: C, 42.62; H, 2.39; N, 8.20; S, 9.49. IR (KBr, cm<sup>-1</sup>): 1578 s  $\nu_{(C=N-N=C)}$ , 1240 s  $\nu_{(C-O)}$ . UV-Vis in DMF:  $\lambda_{max}/nm$  ( $\epsilon_{max}/dm^3mol^{-1}cm^{-1}$ ) 265(80,720) (intra-ligand transition), 365(11252) (LMCT), 426 (2559) (forbidden d→d transition). ESI-MS: m/z 682.70

#### [Ni (L4)<sub>2</sub>] (4)

Color: Orange. Yield: 97.05%. M.P. 352°C; Anal. Calc. for  $C_{26}H_{22}N_4S_2O_4Ni$  (574.41 g mol<sup>-1</sup>): C, 54.36; H, 3.86; N, 9.75; S, 11.16. Found: C, 54.30; H, 3.83; N, 9.78; S, 11.14. IR (KBr, cm<sup>-1</sup>): 1520 s  $\nu_{(C=N-N=C)}$ , 1250 s  $\nu_{(C-O)}$ . UV-Vis in DMF:  $\lambda_{max}/nm$  ( $\epsilon_{max}/dm^3mol^{-1}cm^{-1}$ ) 272(80,470) (intra-ligand transition), 367(11187) (LMCT), 422 (2422) (forbidden d→d transition). ESI-MS: m/z 577.48

### X-ray crystallography

Single crystals of complex **4** suitable for X-ray diffraction analysis was grown by slow evaporation of dimethyl formamide solution of the complexes at room temperature. The data collection was carried out using Bruker SMART APEX II single crystal X-ray diffractometer using monochromated Mo K $\alpha$  radiation ( $\lambda = 0.71073$  Å). The absorption corrections were performed by multi-scan method using SADABS software.<sup>38</sup> Corrections were made for Lorentz and polarization effects. The structures were solved by SIR92 and refined by full-matrix least squares on F<sup>2</sup> using SHELXL 97.<sup>39</sup> All non-hydrogen atoms were refined anisotropically and the hydrogen atoms in these structures were located from the difference Fourier map and constrained to the ideal positions in the refinement procedure. The unit cell parameters were determined by the method of difference vectors using reflections scanned from three different zones of the reciprocal lattice. The intensity data were measured using  $\omega$  and  $\phi$  scan with a frame width of 0.5°. Frame integration and data reduction were performed using the Bruker SAINT-Plus (Version 7.06a) software.<sup>40</sup> The crystal structure and structure refinement parameters for the complex is given in the Table 1.

### DNA binding studies

The experiments involving the binding of compounds with CT-DNA were done in double distilled water with Tris 5mM and sodium chloride 50mM and adjusted the p<sup>H</sup> to 7.2 with hydrochloric acid. A solution of CT-DNA in the buffer gave a ratio of UV absorbance about 1.9 at 260 and 280 nm,

suggesting that the DNA was sufficiently free from protein. The concentration per nucleotide was determined by electronic spectroscopy using a molar extinction coefficient of  $6600 \text{ M}^{-1} \text{ cm}^{-1}$  at 260 nm. The complexes were dissolved in a combined solvent of 5% DMF and 95% Tris-HCl buffer for all of the experiments. A stock-solution of CT-DNA was stored at 277K and used after no more than 4 days. In electronic absorption titration experiments were performed by keeping the fixed concentration of metal complex as constant (25  $\mu\text{M}$ ) and varying the nucleotide concentration (0-60  $\mu\text{M}$ ). Although doing the absorption spectra, equal amounts of DNA were added to both complexes and reference solutions to eliminate the absorbance of DNA itself. Samples were equilibrated before recording each spectrum.

Further support for the binding of complexes to DNA via intercalation was studied by using fluorescence spectral technique in order to find out whether the compound can displace EB from its DNA-EB complex. Ethidium bromide displacement experiments were done by adding the solution of the complexes to the Tris-HCl buffer solution ( $\text{p}^{\text{H}}$ , 7.2) of DNA/EB mixture. DNA was pretreated with ethidium bromide in the ratio  $[\text{DNA}]/[\text{EB}]=10$  for 30 min at 27 °C, then the test solution were added to this mixture of EB-DNA, and the change in the fluorescence intensity was measured. The excitation wavelength 545 nm was fixed for EB bound to DNA were recorded with an increasing amount of the nickel(II) complexes concentration and the emission range was adjusted before measurements. The metal complexes (0-60 $\mu\text{M}$ ) were then added to this mixture and their effect on the emission intensity was measured.

#### Cyclic voltammetry

Electrochemical studies were done on electro chemical analyser CH INSTRUMENTS and the experiments were carried out in a three electrode system comprising a glassy carbon working electrode, a platinum wire auxiliary/counter electrode and a saturated calomel reference (SCE) electrode was used as the reference electrode. The cyclic voltammograms of the complexes were recorded in DMF solutions and in the buffer (5 mM Tris-HCl/ 50 mM NaCl,  $\text{p}^{\text{H}}$  7.2) solution was used as supporting electrolyte at the scan rate 100  $\text{mVs}^{-1}$  TBAP and buffer solution were the supporting electrolytes, respectively. Oxygen was eliminated by purging the solutions with pure which had been previously saturated with solvent vapours. The electrode surface were freshly polished with alumina powder and washed clearly with double distilled water after each polishing step. All electrochemical measurements were performed at  $25.0 \pm 0.2^\circ\text{C}$ .

#### Circular dichroism

Circular dichroism is a useful techniques on how the conformation of the CT-DNA chain altered by the bound complex. A solution of CT-DNA display a positive band (275 nm) from base stacking interactions and a negative band (245 nm) from the right-handed helicity of DNA.<sup>41</sup> The conformational changes are tested by upon the addition of complexes (20  $\mu\text{M}$ ) with DNA concentration at 60  $\mu\text{M}$  in Tris-HCl buffer medium. The spectrum of control DNA and the

complexes was monitored from 220 to 320 nm. Classical intercalation reactions tend to increase the intensities of both bands due to strong base stacking interactions of stable DNA conformations (right-handed B conformations of CT-DNA), whereas simple groove binding and electrostatic interactions with small molecules show small of a perturbation or no perturbation whatsoever on the base stacking and helicity bands.<sup>42</sup>

#### Viscosity Experiments

Viscosity experiments were done by using an ubbelodhe type viscometer at constant temperature at  $29.0 \pm 0.1^\circ\text{C}$  in a thermostatic waterbath. Calf thymus DNA sample solutions were prepared by sonication in order to minimize complexities arising from DNA flexibility.<sup>43</sup> The CT-DNA solution (5  $\mu\text{M}$ ) was titrated with nickel (II) benzhydrazone complexes (0.5-5  $\mu\text{M}$ ), following the variation of the viscosity in each case. Flow time was measured with a digital stopwatch and each sample was measured at least for three times, and an average flow time was calculated. Data are presented as  $(\eta - \eta_0)^{1/3}$  versus binding ratio, where  $\eta$  is the viscosity of DNA in the presence of the complex, and  $\eta_0$  is the viscosity of DNA alone. The relative viscosity values was determined according to the equation  $\eta = (t - t_0)/t_0$ , where  $t_0$  is the total flow time for the buffer and  $t$  is the observed flow time for DNA in the presence and absence of the complex.<sup>44</sup>

#### Protein binding studies

Protein binding study of nickel(II) hydrazone complexes with bovine serum albumin (BSA) was investigated using fluorescence spectra were recorded with an excitation at 280 nm and the emission wavelength at 345 nm corresponding to that of free bovine serum albumin (BSA). The excitation and emission slid widths and scan rates were constantly maintained for all the experiments. Samples were precisely degassed using pure nitrogen gas for 15 minutes by using quartz cells (4 $\times$ 1 $\times$ 1cm) with high vacuum Teflon stopcocks. Stock solutions of BSA was prepared in 50mM phosphate buffer ( $\text{p}^{\text{H}}$ , 7.2) and stored in dark at 4 $^\circ\text{C}$  for additional use. Concentrated stock solutions of metal complexes were prepared by dissolving them in DMF: phosphate buffer (5:95) and diluted suitably with phosphate buffer to get appropriate concentrations. A 2.5 mL solution of BSA (1  $\mu\text{M}$ ) was titrated by consecutive additions of a 25 $\mu\text{L}$  stock solution of complexes ( $10^{-3} \text{ M}$ ) using a micropipette. Synchronous florescence spectra was also studied using the same concentration of BSA and complexes as considered above with two different  $\Delta\lambda$  (difference between the excitation and emission wavelengths of BSA) values such as 15 and 60 nm.

#### Protein cleavage experiments

Protein cleavage experiments were done by incubating BSA (20  $\mu\text{M}$ ) with 1-4 in Tris-HCl buffer for 4h at 37 $^\circ\text{C}$  according to the literature.<sup>45</sup> The samples were dissolved in the loading buffer (24  $\mu\text{L}$ ) containing SDS (7% w/v), glycerol (4%v/v), Tris-HCl buffer (50 mM,  $\text{p}^{\text{H}}$  7.2), mercaptoethanol (2%v/v) and bromophenol blue (0.01% w/v). The protein solutions were then denatured on heating to boil for 3 min. The samples were then loaded on a 3% polyacrylamide (stacking) gel.

Geoelectrophoresis was done beginning at 60 V until the dye passed into the separating gel (12% polyacrylamide) from the stacking (3%) gel, followed by setting the voltage to 110 V for 1.5 h. Staining was done with a Coomassie Brilliant Blue R-250 solution (acetic acid–methanol–water = 1: 2: 7 v/v) and destaining was done with a water–methanol–acetic acid mixture (5: 4: 1v/v) for 4 h. The gels, after destaining, were scanned with a Precision Scan LTX scanner and the images were further processed by using the Adobe Photoshop 7.0 software package.

#### Antioxidant activity

The DPPH (2-2' diphenyl-1-picrylhydrazyl) radical scavenging activity of the compounds was measured according to the method described by Blios.<sup>46</sup> The DPPH radical is a stable free radical having  $\lambda_{\text{max}}$  at 517 nm. The various concentrations (10-50  $\mu\text{M}$ ) of the test compounds was added to a solution of DPPH (125  $\mu\text{M}$ , 2mL) in methanol and the final volume was made upto 4 mL with double distilled water. The solution was incubated at 37°C for 30 min in dark. The decrease in absorbance of DPPH was measured at 517 nm. The same experiment carried out without the test compounds serve as a control.

The hydroxyl radical produced by the  $\text{Fe}^{3+}$ /ascorbic acid system, were detected according to the Nash method<sup>47</sup>. The detection of hydroxyl radicals was done by measuring the amount of formaldehyde produced from the oxidation reaction with DMSO. The formaldehyde produced was detected spectrophotometrically at 412 nm. A mixture of 1.0 mL of iron-EDTA solution (ferrous ammonium sulphate (0.331mM) and EDTA(0.698mM), 0.5 mL of EDTA solution(0.048 mM) and 1.0 mL of DMSO(10.08mM)DMSO(v/v)in 0.1 M phosphate buffer  $\text{p}^{\text{H}}$  7.4) were sequentially added to the test tubes containing the test compounds with different concentrations in the range of 10-50  $\mu\text{M}$ . The reaction mixture contained EDTA (0.1 mM),  $\text{Fe}^{3+}$  (167  $\mu\text{M}$ ), DMSO (33 mM) in phosphate buffer (50 mM,  $\text{p}^{\text{H}}$  7.4), the tested compounds with various concentrations in the range of 10-50  $\mu\text{M}$ . The reaction was initiated by adding 0.5 mL of ascorbic acid (1.25 mM) and incubated 80-90 °C for 15 min in a water bath. After incubation, the reaction was terminated by the addition of 1.0 mL ice cold Trichloroacetic acid (TCA) (107 mM). Subsequently, 3.0 mL Nash reagent was added to each tube and left at room temperature for 15 min. The reaction mixture without sample was used as control. The intensity of the colour formed was measured spectrophotometrically at 412 nm against reagent blank.

Nitric Oxide (NO) radical scavenging activity was determined based on the reported method, when sodium nitroprusside in aqueous solution at physiological  $\text{p}^{\text{H}}$  spontaneously generates nitric oxide, which interacts with oxygen to produce nitrate ions that can be estimated using Griess reagent.<sup>48</sup> For the experiment, sodium nitroprusside (10 mM) in Phosphate buffer saline was mixed with the test compounds at different concentrations in the range of 10-50  $\mu\text{M}$  and incubated at room temperature for 150 min. The reaction without the sample but the equivalent amount of

solvent served as the control. After the incubation period, 0.5 mL of Griess reagent containing sulphanilamide (5.8 mM),  $\text{H}_3\text{PO}_4$  (20mM) and N-(1-naphthyl) ethylene diamine dihydrochloride (0.39 mM) was added mixed to allow standing for 30 min at 25°C. The absorbance of pink coloured chromophore formed during diazotization was measured at 546 nm.

For the above three assay. All the tests were run in triplicate, and various concentrations of the complexes were used to fix a concentration at which the complexes showed around 50% activity. The percentage activity was calculated by using the formula, % of suppression ratio =  $[(A_0 - A_c)/A_0] \times 100$ , where  $A_0$  and  $A_c$  represent the absorbance in the absence and presence of the test compounds respectively. The 50% activity ( $\text{IC}_{50}$ ) can be calculated using the percentage of activity.

#### *In vitro* anticancer activity: Maintenance of cell lines

The cell viability was evaluated by 3-(4, 5-dimethyl thiazol-2yl)-2, 5-diphenyl tetrazolium bromide (MTT) assay, which determines the metabolically active of mitochondria cells.<sup>49</sup> Cells were plated in their growth medium at a density of 5000 cells per well in 96 flat bottomed well plates at plating density of 10,000 cell/well and incubated to allow for cell attachment at 37°C, under conditions of 5%  $\text{CO}_2$ , 95% air and 100% relative humidity. After 24 h the cells were treated with serial concentration of the test samples. The compounds were initially dissolved in neat DMF and an aliquot sample solution was diluted to twice the desired final maximum test concentration with serum free medium. Additional four serial dilutions were made to provide a total of five sample concentrations. Aliquots of 100  $\mu\text{L}$  of these different sample dilutions were added to the appropriate wells already containing 100  $\mu\text{L}$  of medium, resulting in the required final sample concentrations. Following sample addition, the plates were incubated for an additional 48 h at 37 °C 5%  $\text{CO}_2$ , 95% air and 100% relative humidity. The medium containing without samples were served as control and triplicate was maintained for all concentrations.

#### MTT assay

3-[4, 5-dimethylthiazol-2-yl] 2, 5-diphenyltetrazolium bromide (MTT) is a yellow water soluble tetrazolium salt. A mitochondrial enzyme in living cells, succinate dehydrogenase, cleaves the tetrazolium ring, converting the MTT to an insoluble purple formazan. Thus, the amount of formazan produced is directly proportional to the number of viable cells. After 48 h incubation, 15  $\mu\text{L}$  of MTT (5 mg  $\text{mL}^{-1}$ ) in phosphate buffered saline (PBS) was added to each well and incubated at 37 °C for 4h.

The quantity of formazan formed gave a measure of the number of viable cells. HeLa, MCF-7, and NIH 3T3 were used for the MTT assay. The absorbance was monitored at 570 nm (measurement) and 630 nm (reference) using a 96 well plate reader (Bio-Rad, Hercules, CA, USA). Data were collected for four replicates each and used to calculate the respective means. The percentage of inhibition was calculated, from this data, using the formula:

$$\% \text{ cell inhibition} = 1 - \frac{\text{Abs (sample)}}{\text{Abs (control)}} \times 100$$

The  $IC_{50}$  value was calculated as the complex concentration that is required to reduce the absorbance to half that of the control.

#### Neutral Red Uptake Assay

This test was performed according to well known standard methods.<sup>50</sup> Cells were plated in 96 well plates (40,000 cells per well) and incubated in DMEM+ 10% FBS for 24 hours at 37 °C and 5% CO<sub>2</sub>. The complexes were then added in different concentrations for additional 24 hours. Cells were then washed with PBS after which 200  $\mu$ L of a 0.625  $\mu$ g/ml neutral red solution was added. After 3h cells were again washed in PBS to remove the remaining dye. Addition of 200  $\mu$ L ethanol/acetic acid (50/1) resulted in release of the dye from the cells that were placed in a shaking bath until a homogeneous colour was formed (approx.1h). The optical density was measured with a spectrometer at 540 nm.

#### Fluorescent dual staining experiment

Acridine Orange and Ethidium Bromide (AO and EB) staining was performed as follows: the cell suspension of each sample containing 5  $\times 10^5$  cells, was treated with 25  $\mu$ L of AO and EB solution (1 part of 100  $\mu$ g mL<sup>-1</sup> AO and 1 part of  $\mu$ g mL<sup>-1</sup> EB in PBS) and examined at 20x magnifications in a laser scanning confocal microscope LSM 710 (Carl Zeiss, Germany) using an UV filter (450–490 nm). Three hundred cells per sample were counted in triplicate for each dose point. The cells were scored as viable, apoptotic or necrotic as judged by the staining, nuclear morphology and membrane integrity. Morphological changes were also observed and photographed.

#### DAPI staining method

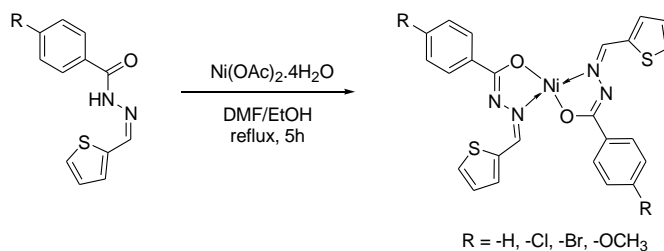
DAPI (4', 6'-diamidino-2- phenylindole) staining was carried out by using the following procedure: 5  $\times 10^5$  cells were treated with the complex (100  $\mu$ g mL<sup>-1</sup>) for 24 h in a 6-well culture plate and were fixed with 4% paraformaldehyde followed by permeabilization with 0.1% Triton X-100. Cells were then stained with 50  $\mu$ g mL<sup>-1</sup> DAPI for 30 min at room temperature. The cells undergoing apoptosis, represented by the morphological changes of apoptotic nuclei, were observed and imaged from ten eye views at 20x magnifications under a laser scanning confocal microscope LSM 710 (Zeiss).

#### Apoptosis evaluation - Flow cytometry

The cells were grown in 6 well plates and exposed to three different concentrations of nickel(II) benzhydrazone complex 4 for 48 h. The Annexin V-FITC kit uses annexin V conjugated with fluorescein isothiocyanate (FITC) to label phosphatidylserine sites on the membrane surface of apoptotic cells. Briefly the cells were trypsinised and washed with Annexin binding buffer and incubated with Annexin V FITC and PI for 30 minutes and immediately analysed using flow cytometer FACS Aria-II. The results were analysed using DIVA software and percentage positive cells were calculated.

## Results and Discussion

The benzhydrazone ligand derivatives were prepared in high yield by the condensation of thiophene aldehydes with substituted benzhydrazides in an equimolar ratio. These ligands were allowed to react with the (CH<sub>3</sub>COO)<sub>2</sub>Ni·4H<sub>2</sub>O in a 1:2 molar ratio in DMF/ethanol medium under reflux for 5h afforded in the formation of new square planar nickel(II) benzhydrazone complexes of the formula [Ni(L)<sub>2</sub>] (Scheme1). In this reaction the acetate anion acts as the base and promotes the formation of these complexes. The oxidation state of nickel remains unchanged during the formation of the complex. All the complexes are orange in colour, air stable in both the solid and the liquid states at room temperature and are non-hygroscopic. The synthesized nickel(II) benzhydrazone complexes are sparingly soluble in solvents such as chloroform, dichloromethane or acetonitrile and are readily soluble only in solvents such as dimethyl formamide (DMF) and dimethyl sulphoxide (DMSO) producing intense orange coloured solutions. The analytical data of all the nickel(II) benzhydrazone complexes are in good agreement with the molecular structures proposed.



**Scheme 1** Synthesis of nickel(II) benzhydrazone complexes.

The IR spectra of the free ligands showed a medium to strong band in the region 3254-3296 cm<sup>-1</sup> which is characteristic of the N-H functional group. The free ligands also display  $\nu_{C=N}$  and  $\nu_{C=O}$  absorptions in the region 1636-1644 cm<sup>-1</sup> respectively indicating that the ligand exists in amide form in solid state. The bands due to  $\nu_{N-H}$  and  $\nu_{C=O}$  stretching vibrations are not observed in the complexes indicating that the ligand undergo tautomerization and subsequent coordination of the imidolate enolate form during complexation. Coordination of the ligand to the nickel(II) ion through azomethine nitrogen is expected nitrogen is expected to reduce the electron density in the azomethine link and thus lowers the absorption frequency after complexation (1520-1583 cm<sup>-1</sup>), indicating the coordination of azomethine nitrogen to the nickel(II) ion. The presence of a new band in the region 440-470 cm<sup>-1</sup> due to  $\nu(Ni-N)$  is another indication of the involvement of nitrogen of the azomethine group in coordination.<sup>52</sup> The band 1238-1250 cm<sup>-1</sup> in the region is due to the imidolate oxygen is coordinated to the metal.<sup>53</sup> The IR spectra of all the complexes therefore confirm the coordination mode of the benzhydrazone ligand to the nickel(II) ion via the azomethine nitrogen and imidolate oxygen.

The absorption spectra of all the nickel(II) benzhydrazone complexes 1-4 were recorded in dimethyl formamide solution

in the range 200–800 nm at room temperature and all the complexes showed three bands with absorption maxima in the region 265–426 nm and shown in Fig. S1–S4 (ESI<sup>†</sup>). The electronic spectrum of the hydrazone ligand in DMF solution showed two broad absorption bands at 268 and 323 nm corresponds to  $\pi$ – $\pi^*$  and  $n$ – $\pi^*$  transitions. The former band is due to  $\pi$ – $\pi^*$  transitions within the aromatic rings and remains almost unchanged in the spectra of metal complexes, while the second band, due to  $n$ – $\pi^*$  transition within the  $>C=N-N$  chromophore, is shifted to a longer wavelength as a consequence of coordination when binding with the metal atom, confirming the formation of metal complexes and reflecting the azomethine nitrogen is involved in coordination.<sup>54</sup> The UV-Vis spectra of the nickel(II) complexes the bands in the region of 265–272 nm which corresponds to ligand-centered (LC) transition. The other high intensity band has been assigned in the region 361–365 nm is due to charge transfer (LMCT) nitrogen-metal absorption band. The longer wavelength band in the region of 421–426 nm corresponds to the d-d transitions of a  $d^8$  low-spin  $Ni^{II}$  in slightly distorted square-planar geometry.

The <sup>1</sup>H NMR spectrum of the complexes in DMSO gave very broad signals, suggesting that ligand exchange takes place in DMSO solution. However, we have recorded mass spectra for all the complexes which confirm the formation of nickel(II) benzhydrazone complexes and shown in Fig. S5–S8 (ESI<sup>†</sup>). Mass spectrometric measurements carried out under positive/negative-ion ESI conditions with different cone voltages, using DMF as the solvent and the mobile phase. The ESI spectra of complexes 1 and 2 exhibit base peaks at  $m/z$  522.85 and  $m/z$  592.57 respectively while the complexes 3 and 4 display base peaks at  $m/z$  682.70 and  $m/z$  577.48 respectively.

### Single crystal X-ray crystallography

Attempts were made to grow single crystals for X-ray diffraction to confirm the molecular structures and geometry of all the synthesised complexes. But we could not succeed in getting single crystals except for complex 4 [Ni(L4)<sub>2</sub>] due to solubility problem. The crystal structure of the complex 4 is shown in Fig.1 and pertinent crystallographic data are listed in Table 1. The complex crystallizes in the  $P2_1/c$  space group. The nickel ion is tetra-coordinated in square planar geometry by two benzhydrazone ligand molecules acting as monoanionic bidentate N, O-donor via azomethine nitrogen and the deprotonated amide oxygen in the benzhydrazone fragment, forming two fused five-membered chelate rings. The ligand is trans position with respect to C–N bond and the complex is centrosymmetric around the nickel center. Nickel is therefore sitting in a  $N_2O_2$  coordination environment, which is square planar in nature as unveil in all the bond parameters around nickel. In the complex benzhydrazone ligand binds with metal center at N and O forming two five membered chelate ring with bite angle  $N(1)–Ni(1)–O(1)$   $96.1(1)^\circ$  and  $O(1)–Ni(1)–N(1)$   $83.9(1)^\circ$ . The bond lengths of  $Ni(1)–N(1)$  and  $Ni(1)–O(1)$  are 1.850(2) and 1.838(2) Å respectively. The bond lengths and

bond angles are in good agreement with reported data on related nickel(II) complexes with square planar geometry.<sup>55</sup> As all the four nickel(II) complexes exhibit similar spectral properties, the other three complexes are considered to have a similar structure to that of complex 4. The X-ray determination confirms the structure proposed on the spectroscopic data, consistent with metal bivalency and the mono ionised nature of the ligand in complexes.

**Table 1** Crystal data and structure refinement of the complex 4

Empirical formula	C <sub>26</sub> H <sub>22</sub> N <sub>4</sub> O <sub>4</sub> S <sub>2</sub> Ni
Formula weight	577.29
Colour	Orange
Temperature (K)	296(2)
Wavelength (Å)	MoK $\alpha$
Crystal system	Monoclinic
Space group	$P2_1/c$
a (Å)	13.5191(10)
b (Å)	5.4599(4)
c (Å)	18.3237(14)
$\alpha$ (°)	90.00
$\beta$ (°)	108.169(4)
$\gamma$ (°)	90.00
Volume (Å <sup>3</sup> )	1285.09(17)
Z	2
D <sub>cal</sub> (Mg/m <sup>3</sup> )	1.431
Absorption Coefficient (mm <sup>-1</sup> )	1.012
F(000)	532
Crystal size (mm)	0.54×0.09×0.09
Theta range (°)	1.59–30.39
Limiting Indices	$-19 \leq h \leq 19$ , $-7 \leq k \leq 4$ ,
Reflections collected	12482
Independent reflections	3830
Data/restraints/parameters	3830/0/71
Goodness-of-fit (GOF) on F <sup>2</sup>	1.041
Final R indices [ $I > 2\sigma(I)$ ]	$R_1 = 0.0545$ , $wR_2 = 0.1512$
R indices (all data)	$R_1 = 0.1151$ , $wR_2 = 0.1159$
R <sub>int</sub>	0.0463
Largest diff. peak and hole eÅ <sup>-3</sup>	0.656 and -0.778

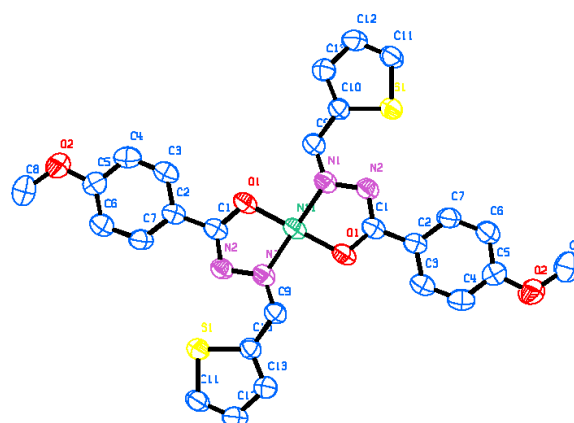


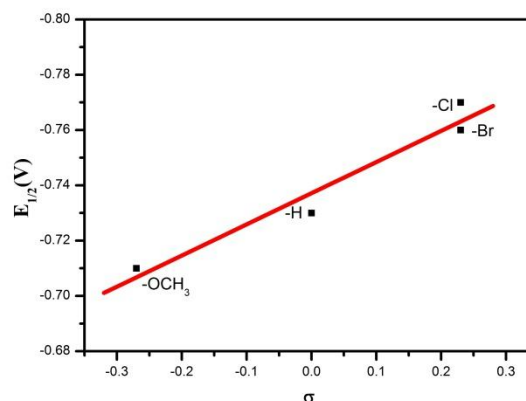
**Fig. 1** The molecular structure of the complex-4 (hydrogen atoms are omitted for clarity; displacement parameters are drawn at 50% probability level).

**Table 2** Selected bond lengths (Å) and bond angles (°) for complex-4

Complex	4
Ni (1) –O(1)	1.838(2)
Ni(1) –N(1)	1.850(2)
O(1) – C(1)	1.306(3)
O(2) – C(5)	1.358(3)
O(1) – C(8)	1.420(5)
S(1) – C(10)	1.724(2)
S(2) – C(11)	1.703(4)
N(1) – N(2)	1.379(3)
N(1) – C(9)	1.300 (4)
N(2) – C(1)	1.317(4)
O(1) – Ni(1) – O(1)	180.0(9)
N(1) – Ni(1) – N(1)	180.0(1)
O(1) – Ni(1) –N(1)	83.9(1)
N(1) – Ni(1) – O(1)	96.1(1)
N(1) – N(2)- C(1)	108.2 (2)
S(1) – C(10)-C(13)	110.8 (2)
Ni (1) – O(1)-C(1)	110.9(2)
Ni(1) - N(1)-N(2)	114.4 (2)
N(1)-C(9) -H(9)	116.3 (3)
N(2)-N (1)-C(9)	116.6 (2)
N(2)-C (1) -C(2)	119.1 (3)
O(1)-C(1) -N(2)	122.6(3)
S (1) – C(10)- C(9)	125.6 (2)
Ni(1) - N(1)- C(9)	129.1 (2)
O(1) – Ni(1)-N(1)	96.1(1)

### Electron transfer property

Electrochemical studies were carried out for all the free ligands and the nickel(II) benzhydrazone complexes in DMF solution under an atmosphere of nitrogen in the potential range of +1.4 to –1.4 V. 0.05 M tetrabutylammonium perchlorate (TBAP) was used as the supporting electrolyte and the concentration of the complexes were  $\sim 10^{-3}$  M. The potentials of all the nickel(II) benzhydrazone complexes are summarized in Table 3 and cyclic voltammogram of all the complexes are shown in Fig. S9-S12 (ESI<sup>+</sup>). We have not observed any redox waves within the potential limits of +1.4 to –1.4 V for free ligands and hence whatever the responses observed within this potential limits were due to metal centre only. All the complexes display a quasi reversible reduction ( $\text{Ni}^{\text{II}} \rightarrow \text{Ni}^{\text{I}}$ ) at a scan rate of 100  $\text{mV s}^{-1}$ . The single-electron nature of the voltammograms has been confirmed by the comparison of current heights for the complexes and that of a simple  $[\text{Fe}(\text{bipy})_3]^{2+}$  complex under identical conditions.<sup>56</sup> All the complexes showed well-defined reduction waves with  $E_{1/2}$  in the range of –0.71 to –0.77 V. The redox processes are quasi-reversible in nature, characterized by a rather large peak-to-peak separation ( $\Delta E_p$ ) of 210–310 mV.<sup>57</sup> The redox potentials are virtually independent of scan rates, indicating quasi-reversibility.<sup>58</sup> In general, the reason for the quasi-reversible electron transfer in the above complexes may be either due to the slow electron transfer or the deposition of the complex on the electrode surface.

**Fig. 2** Least Square Plot of  $E_{1/2}$  values reduction ( $\text{Ni}^{\text{II}}/\text{Ni}^{\text{I}}$ ) potential vs  $\sigma$ .

The potential of reduction  $\text{Ni}^{\text{II}}/\text{Ni}^{\text{I}}$  has been found to be sensitive to the nature of the substituent R in the thiophene aldehyde benzhydrazone ligand which perturbs the metal reduction. The potential increases linearly with increasing electron-withdrawing character of R. The plot of formal potential  $E_{1/2}$  versus  $\sigma$  (where  $\sigma$  is Hammett substituent constant<sup>59</sup> of R;  $\sigma$  values for R:  $\text{OCH}_3 = -0.27$ ,  $\text{H} = 0.00$ ,  $\text{Cl} = +0.23$ ,  $\text{Br} = +0.23$ ) is found to be linear for the reduction couples are shown in Fig. 2. The slope of this line which is known as the reaction constant,  $\rho$ , is the measure of the sensitivity of  $E_{1/2}$  with the substituent (R) for the  $\text{Ni}^{\text{II}}/\text{Ni}^{\text{I}}$  couple. This shows that the nature of the para substituent R on the thiophene aldehyde benzhydrazone ligands can still influence the metal-centered potentials in a predictable manner.

**Table 3** Cyclic voltammetry data of the nickel(II) benzhydrazone complexes

Complexes	$E_{pc}$ (V)	$E_{pa}$ (V)	$E_{1/2}$ (V)	$\Delta E_p$ (mV)
1	-0.87	-0.58	-0.73	290
2	-0.88	-0.67	-0.77	210
3	-0.89	-0.62	-0.76	270
4	-0.87	-0.56	-0.71	310

Solvent = Dimethyl formamide; [Complex] =  $1 \times 10^{-3}$  M; Supporting electrolyte:  $[\text{Bu}_4\text{N}](\text{ClO}_4)$  (0.05 M); Scan rate: 100  $\text{mV s}^{-1}$ ;  $E_{pa}$  and  $E_{pc}$  = anodic and cathodic peak potentials respectively;  $E_{1/2} = 0.5(E_{pc} + E_{pa})$ ;  $\Delta E_p = (E_{pc} - E_{pa})$ ; All potentials referenced to SCE.

### DNA-binding studies

DNA is the primary pharmacological target of many antitumor compounds. DNA-metal complex interaction has paramount importance in understanding the mechanism of tumour inhibition for the treatment of cancer. The interaction of nickel (II) benzhydrazone complexes 1-4 with CT-DNA was studied by a number of techniques, such as absorption spectral titration,

fluorescence spectroscopy, cyclic voltammetry, and circular dichroism and viscosity measurements.

#### UV-Vis absorption studies

Electronic absorption spectroscopy is commonly employed to determine the binding ability of metal complexes with DNA helix. Complexes that bound to DNA through intercalation are characterised by a change in absorbance (hypochromism) and bathochromic shift in wavelength, due to a strong stacking interaction between the aromatic chromophore of the test complexes and DNA base pairs.<sup>60</sup> The extent of hypochromism is commonly consistent with the strength of intercalative intercalation.<sup>61</sup> The interaction of the complexes with CT-DNA was followed by recording the UV-visible spectra of the system. The experiment was carried out keeping the concentration of the nickel(II) benzhydrazone complexes (25  $\mu\text{M}$ ) as constant and changing the concentration of the CT-DNA (0–60  $\mu\text{M}$ ). The absorption bands at 273 nm and 321 nm in the complexes were considered for the corresponding adsorptivity changes upon the incremental addition of CT-DNA.

The absorption spectra of complexes 1–4 in the absence and presence of CT-DNA are shown in Fig.3. From the electronic absorption spectral data, it was clear that increasing the concentration of DNA added to the nickel(II) complexes 1–4 all of the above mentioned absorption bands showed hypochromism accompanied with 34.14%, 34.82%, 34.05% and 41.92% bathochromic shift of 2–3 nm show that the nickel(II) benzhydrazone complexes bind strongly to CT-DNA *via* the intercalative mode. The observed hypochromism is due to stacking interaction between the aromatic chromophores of the complexes and DNA base pairs consistent with the intercalative mode of binding. These observations are similar to those reported earlier for various metallointercalators.<sup>62</sup> To compare the binding strength of the complexes with CT-DNA, the intrinsic binding constant  $K_b$  have been determined from the equation (1):

$$[\text{DNA}]/[\epsilon_a - \epsilon_f] = [\text{DNA}]/[\epsilon_b - \epsilon_f] + 1/K_b [\epsilon_b - \epsilon_f] \quad (1)$$

Where, [DNA] is the concentration of DNA in base pairs,  $\epsilon_a$  is the extinction coefficient of the complex at a given DNA concentration,  $\epsilon_f$  is the extinction coefficient of the complex in free solution and  $\epsilon_b$  is the extinction coefficient of the complex when fully bound to DNA. A plot of  $[\text{DNA}]/[\epsilon_b - \epsilon_f]$  versus [DNA] gave a slope and intercept equal to  $1/[\epsilon_b - \epsilon_f]$  and  $(1/K_b) [\epsilon_b - \epsilon_f]$ , respectively.  $K_b$  was calculated from the ratio of the slope to the intercept.

The intrinsic binding constant ( $K_b$ ) values were calculated using the above equation and were found to be  $1.60(\pm 0.10) \times 10^5 \text{M}^{-1}$ ,  $2.84(\pm 0.06) \times 10^5 \text{M}^{-1}$ ,  $2.34(\pm 0.08) \times 10^5 \text{M}^{-1}$  and  $3.55(\pm 0.02) \times 10^5 \text{M}^{-1}$  corresponding to the complexes 1–4 respectively. From this experimental result, it is very clearly shows that the increase in electron donating ability of the substituent present in the ligands increases the DNA binding ability of the complexes. The presence of electron withdrawing groups in complex 2 and 3 has almost comparable binding constant value. The complex 1 has lower binding constant may

be due to presence of H as substituent. The electronic absorption titration studies reveals that all the complexes interact with DNA via intercalative mode and complex 4 binds to CT-DNA more strongly than the other complexes. The binding mode needs to be proved by some experiments.

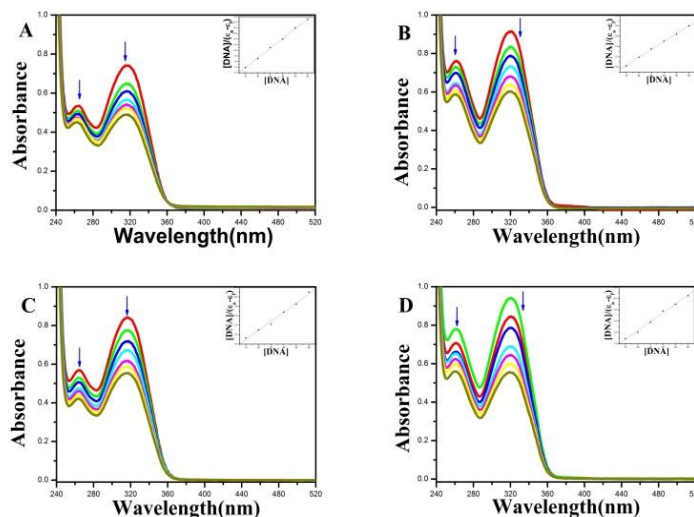


Fig. 3 Electronic absorption spectra of complexes bound to DNA 1(A), 2(B), 3(C) and 4(D) [DNA]= 0–60  $\mu\text{M}$ , [Complex]=25  $\mu\text{M}$  (Inset: plot of  $[\text{DNA}]/\epsilon_b - \epsilon_f$ )/[DNA]).

#### Emission quenching Titration:

EB is a general fluorescent probe for DNA structures and has been engaged in examinations of the mode and process of metal complex binding to DNA. The fluorescent emission of EB bound to DNA in the presence of nickel(II) benzhydrazone complexes are shown in Fig.4. The emission intensity of the EB-DNA system ( $\lambda=595 \text{ nm}$ ) decreased apparently as the concentration of the complexes increased, which indicate that the complexes replace EB from the DNA-EB system. The resulting decrease in fluorescence was caused by EB changing from a hydrophobic environment to an aqueous environment.

The quenching constant has been calculated from the Stern-Volmer equation (2):

$$I_0/I = 1 + K_q [Q] \quad (2)$$

Where  $I_0$  is the emission intensity of the absence of quencher,  $I$  is the emission intensity of the presence of quencher,  $K_q$  is the quenching constant,  $[Q]$  is the quencher concentration.  $K_q$  is the slope obtained from the plot of  $I_0/I$  versus  $[Q]$  (shown as insets in Fig.4). The quenching plots illustrate that the quenching of EtBr bound to CT-DNA by the nickel(II) benzhydrazone complexes are in good agreement with the linear Stern-Volmer equation. The  $K_q$  values are obtained from the experiments are  $1.01(\pm 0.14) \times 10^5 \text{M}^{-1}$ ,  $1.03(\pm 0.10) \times 10^5 \text{M}^{-1}$ ,  $1.03(\pm 0.12) \times 10^5 \text{M}^{-1}$  and  $1.04(\pm 0.08) \times 10^5 \text{M}^{-1}$  respectively. Further the apparent DNA binding constant ( $K_{app}$ ) were calculated from the following equation (3):

$$K_{\text{EtBr}} [\text{EtBr}] = K_{\text{app}} [\text{complex}] \quad (3)$$

(where the complex concentration has the value at a 50% reduction of the fluorescence intensity of EtBr,  $K_{\text{EtBr}} = 1.0 \times 10^7 \text{ M}^{-1}$  and  $[\text{EtBr}] = 10 \mu\text{M}$ ) were found to be  $5.26 \times 10^5 \text{ M}^{-1}$ ,  $5.35 \times 10^5 \text{ M}^{-1}$ ,  $5.81 \times 10^5 \text{ M}^{-1}$ , and  $6.25 \times 10^5 \text{ M}^{-1}$  for complexes **1-4** respectively.

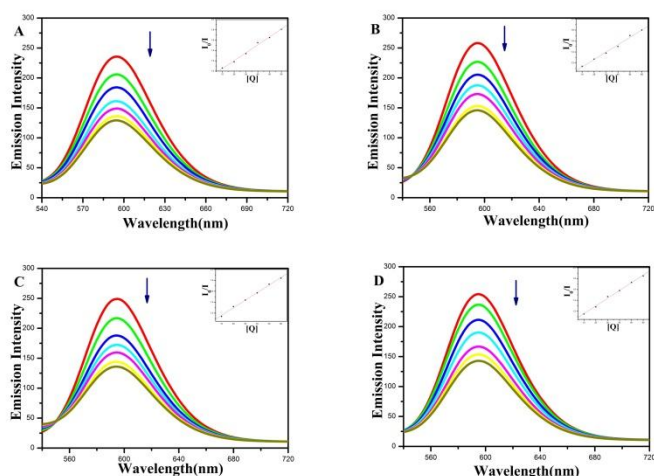


**Fig. 4** The Fluorescence quenching curves of EtBr bound to DNA: **1**(A), **2**(B), **3**(c) and **4**(D),  $[\text{DNA}] = 10 \mu\text{M}$ ,  $[\text{EB}] = 10 \mu\text{M}$ ,  $[\text{Complex}] = 0-60 \mu\text{M}$  (Inset: Plot of  $\log(I_0/I)$  Vs  $[Q]$ ).

The fluorescence quenching spectra of DNA-bound EtBr by complexes **1-4** shown (Fig.4) illustrate that, as the concentration of the complexes increases, the emission band at 595 nm (545 nm excitation) exhibited hypochromism up to 44.85%, 44.53%, 45.73% and 46.20% with hypsochromic shift of 2-3 nm of the initial fluorescence intensity for complexes **1-4** respectively. The observed decrease in the fluorescence intensity clearly reveals that the EtBr molecules are displaced from their DNA binding sites by the complexes under inspection.<sup>63</sup>

#### Cyclic Voltammetry

The different modes of interaction of metal complexes with DNA can be studied not only by electronic absorption spectral studies but also by cyclic voltammetry. In order to investigate the interaction mode between the nickel(II) hydrazone complexes and DNA, cyclic voltammetry experiment was carried out. In general, the electrochemical potential of a small molecule will shift positively when it intercalates into DNA double helix, and it will shift to a negative direction in the case of electrostatic interaction with DNA.<sup>64, 65</sup>

In CV titration both the concentration and volume of the analyte were kept constant while changing the concentration of DNA in solution. Typical CV behaviour of nickel(II) hydrazone complexes  $[\text{Ni}(\text{L}1)_2]$  in the absence and presence of different concentrations of CT-DNA is shown in Fig.5. When CT-DNA is added to a solution of complex both anodic and cathodic peak current heights of the complex decreased in the same manner of increasing additions of DNA. Further during DNA addition the anodic peak potential ( $E_{\text{pa}}$ ), cathodic peak potential ( $E_{\text{pc}}$ ) and  $E_{1/2}$  (calculated as the average of  $E_{\text{pc}}$  and  $E_{\text{pa}}$ ) all showed positive shifts. These positive shifts are considered as evidences for intercalation of complex into the DNA, because

this kind of interaction is due to hydrophobic interaction. From the other point of view, if a molecule binds electrostatically to the negatively charged deoxyribose-phosphate backbone of DNA, negative peak potential should be detected. Therefore, the positive shift in the CV peak potential of the nickel (II) hydrazone complexes is indicative of intercalation binding mode with DNA molecule.<sup>66</sup>

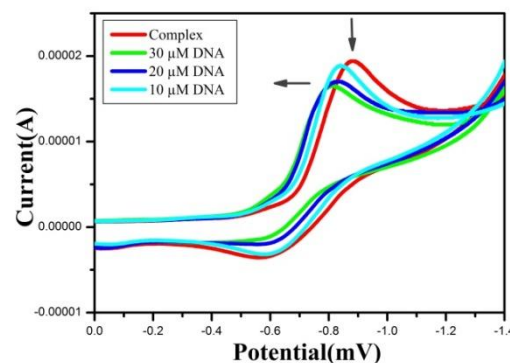


**Fig. 5** Cyclic voltammety measurements at a scan rate 100 mV/s  $[\text{complex}] = 10 \mu\text{M}$  and  $[\text{CT-DNA}]$  addition (0-30  $\mu\text{M}$ ).

#### Circular dichroism spectral study

CD has been effectively used in interpreting the conformational changes of DNA upon metal complex binding. The circular dichroic spectrum of DNA shows a positive band at 275 nm (UV-Vis:  $\lambda_{\text{max}} = 258 \text{ nm}$ ) due to base stacking due to base stacking and negative band at 245 nm due to helicity of B-type DNA.<sup>67</sup> The simple groove binding and electrostatic interaction of the molecules shows small or no perturbation on the base stacking and helicity, although intercalation increases the intensities of both the positive and negative bands. The CD spectrum of CT-DNA (60  $\mu\text{M}$ ) in the presence of complex **1** at (20  $\mu\text{M}$ ) is shown in Fig.6. From the experimental results, we observed the addition of the complexes to the DNA system increased the intensity of both the positive and negative bands of free DNA which is clear information of intercalation between the nickel(II) benzhydrazone complexes and CT-DNA. The CD spectra indicates that the binding of complexes **1-4** to CT-DNA resulting to a significant increases in the intensities of the both positive and negative bands without any shift in peak positions which show that the binding of complexes does not lead to any significant change in the conformation of CT DNA.<sup>61</sup>

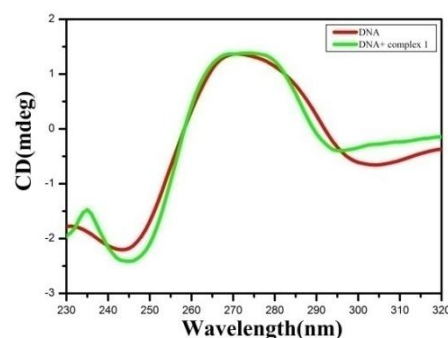


**Fig. 6** Circular dichroic spectrum of CT-DNA (60  $\mu\text{M}$ ) in the presence of complex-**1** (20  $\mu\text{M}$ ).

### Viscosity studies

To further explore the binding of the nickel(II) benzhydrazone complexes, viscosity measurements were carried out on calf thymus DNA by varying the concentration of the added complexes. Optical photo physical probes generally provide necessary but not sufficient clues to support a binding model. Viscosity measurements that are sensitive to length change are regarded as the least ambiguous and the most critical tests of binding model in solution in the absence of crystallographic structural data or NMR.<sup>68</sup> A classical intercalation model results in lengthening the DNA helix, as base pairs are separated to accommodate the binding ligand, leading to the increase of DNA viscosity. However, a partial and/or nonclassical intercalation of ligand may bend or kink the DNA helix, resulting in the decrease of its effective length and, concomitantly, its viscosity.<sup>69</sup>

The effects of the nickel(II) complexes on the viscosity of CT-DNA are shown in the (Figure 7). The values of  $(\eta - \eta_0)^{1/3}$ , where  $\eta$  and  $\eta_0$  are the specific viscosities of DNA in the presence and absence of the complexes are plotted against  $[\text{complex}]/[\text{DNA}]$ . The relative viscosity of CT-DNA exhibits a considerable increase in the presence of increasing amounts of the complexes. Such behaviour indicates that the complex insert between the DNA bases, thus resulting in an intercalative binding mode between DNA and each complex. The ability of the complexes to increase the viscosity of DNA follows the order  $1 < 3 < 2 < 4$ .

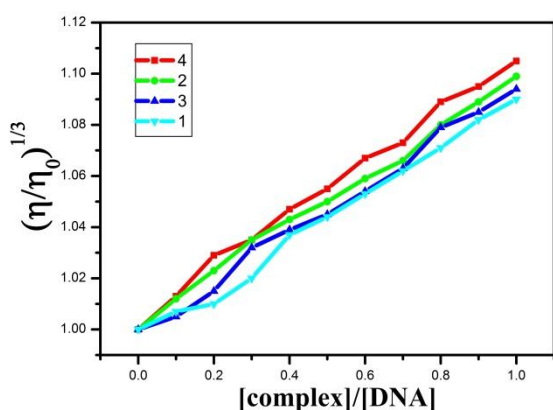


**Fig. 7** Effect of increasing amounts of complexes **1-4** on the relative viscosities of CT-DNA at  $29.0 \pm 0.1^\circ\text{C}$   $[\text{DNA}] = 5\mu\text{M}$  and  $[\text{complexes}] = 0-5\mu\text{M}$ .

### Protein binding studies

#### Fluorescence quenching of BSA by nickel(II) benzhydrazone complexes

It is well-known that the transport of drugs through the blood stream is affected via the interaction of drugs with blood plasma proteins, particularly with serum albumin. An analysis of the binding of chemical compounds to BSA is commonly investigated by examining fluorescence spectra. The binding of BSA with the nickel(II) benzhydrazone complexes was studied by fluorescence measurement at room temperature. Various concentrations of complexes 1-4 were added to the solutions of BSA (1mM), and the fluorescence spectra were recorded in

the range of 300-450 nm upon excitation at 280 nm. The effects of complexes on the fluorescence emission spectrum of BSA are given in Figure 8. Upon the addition of the nickel(II) benzhydrazone complexes to the solution of BSA at 345 nm, up to 40.12, 35.84, 34.64 and 43.06% from the initial fluorescence intensity of BSA, accompanied a hypsochromic shift of 3-5 nm for complexes **1-4**, has been observed respectively.

The observed blue shift is mainly due to the fact that the active site in the protein is buried in a hydrophobic environment. These results suggested a strong interaction of all the complexes with the BSA protein. The fluorescence quenching is described by stern-Volmer relation:

$$I_0/I = 1 + K_{sv} [Q]$$

Where  $I_0$  is the emission intensity of the absence of quencher,  $I$  is the emission intensity of the presence of quencher,  $K_{sv}$  is the Stern-Volmer quenching constant,  $[Q]$  is the quencher concentration.  $K_{sv}$  is the slope obtained from the plot of  $I_0/I$  versus  $[Q]$  (Shown in Fig.8) was found to be  $1.02(\pm 0.04) \times 10^6 \text{ M}^{-1}$ ,  $1.01(\pm 0.07) \times 10^6 \text{ M}^{-1}$ ,  $1.01(\pm 0.18) \times 10^5 \text{ M}^{-1}$  and  $1.02(\pm 0.15) \times 10^6 \text{ M}^{-1}$  corresponding to the complexes **1-4** respectively. It is assumed that the binding of compounds with BSA occurs at equilibrium binding constant can be analysed according to the Scatchard equation.

$$\log [F_0 - F/F] = \log K + n \log [Q]$$

Where,  $K$  and  $n$  are the binding constant and the number of binding sites, respectively. The plot of  $\text{Log} [F_0 - F/F]$  versus  $\text{log} [Q]$  can be used to determine the values of both  $K$  as well as  $n$  and such values calculated for complexes 1-4 shown in Fig.9 are listed in Table 4. From the values of  $n$ , it is clearly showed that there is only one independent class of binding sites for the complexes on BSA and also direct relation between the binding constant and number of binding sites.

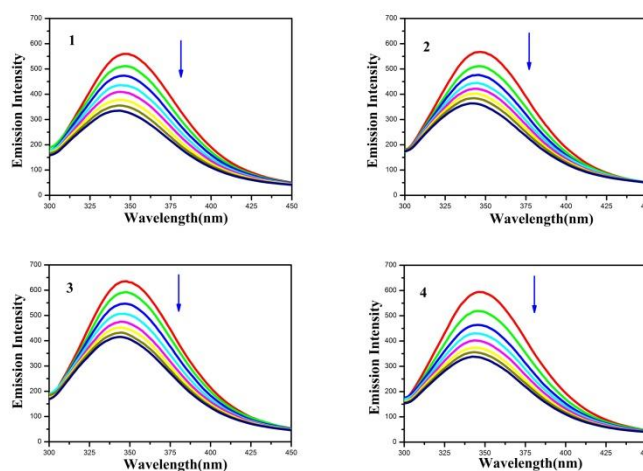


**Fig. 8** The emission spectra of BSA at various concentration of complexes **1-4**  $[\text{BSA}] = 1\mu\text{M}$  and  $[\text{complexes}] = 0-70\mu\text{M}$ .

The larger value of  $K_{bin}$  and  $K_q$  reveals that strong interaction between the BSA and complexes. The calculated value of  $n$  is around 1 for all the complexes indicating the existence of just a single binding site in BSA for all the complexes. The result of binding constant value indicates that the complexes bind to BSA in the order of complexes  $4 > 2 > 3 > 1$ . Complex 4 can interact with the active site by making it more hydrophobic. Among the four nickel(II) benzhydrazone complexes, the complex 4 has stronger interaction with BSA than the other nickel(II) benzhydrazone complexes.

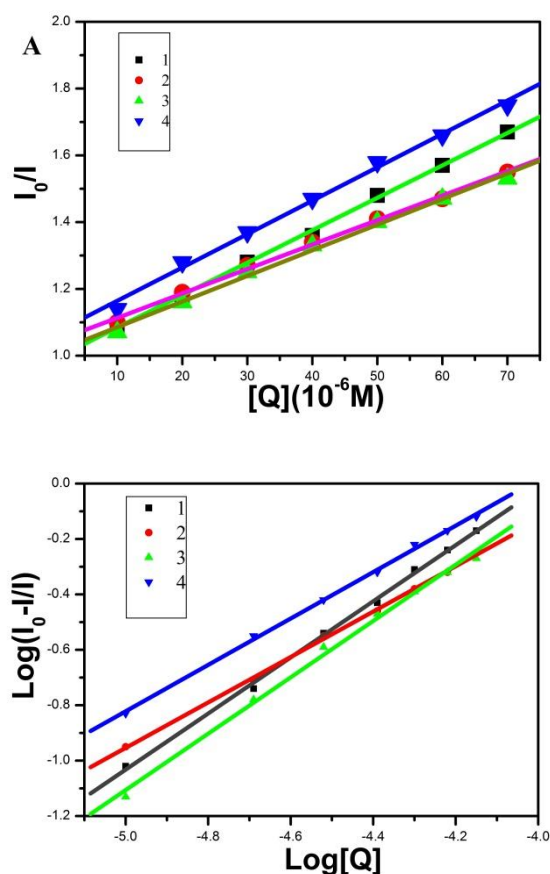


Fig.9 The Stern-Volmer plots (A) and Scatchard plots (B) of the fluorescence titration of complexes 1-4 with BSA.

Table 4 Binding constant and number of binding sites for the interactions of nickel(II) benzhydrazone complexes 1-4 with BSA

System	$K$ ( $M^{-1}$ )	$n$
BSA+ complex 1	$1.07(\pm 0.08) \times 10^6$	$1.01(\pm 0.01)$
BSA+ complex 2	$1.51(\pm 0.04) \times 10^6$	$0.82(\pm 0.05)$
BSA+ complex 3	$1.08(\pm 0.23) \times 10^6$	$1.02(\pm 0.15)$
BSA+ complex 4	$2.40(\pm 0.06) \times 10^6$	$0.84(\pm 0.10)$

### UV-Vis absorption studies

Commonly, quenching occurs through either static or dynamic quenching. The dynamic quenching is a process in which the fluorophore and the quencher come into contact during the transient existence of the excited state, whereas static quenching refers to the formation of fluorophore-quencher complex in the ground state. The simple method to evaluate the type of quenching is UV-visible spectroscopy. Fig.10. shows the UV-vis spectra of BSA in the presence and absence of the complexes, which indicated that the absorption intensity of BSA was enhanced as the complexes were added, and there was a little blue shift of about 2 nm for all the complexes. It revealed the existence of a static interaction between BSA and the complexes.<sup>60</sup>

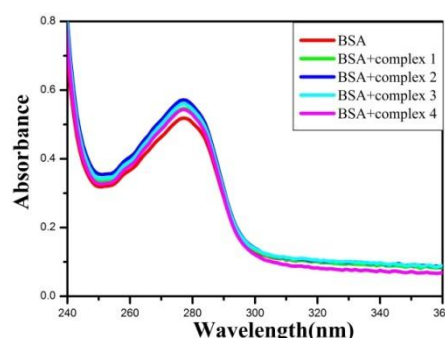


Fig. 10 The absorption spectra of BSA ( $1 \times 10^{-5}$  M) in the presence of complexes 1-4 ( $5 \mu M$ ).

### Characteristics of synchronous fluorescence spectra

It provides information on the molecular environment, particularly in the vicinity of the fluorophore functional groups.<sup>70</sup> It is well known fact that the fluorescence of protein is may be due to presence of tyrosine, tryptophan and phenylalanine residues and hence spectroscopic methods are usually applied to investigate the conformational changes of serum protein. According to Miller,<sup>71</sup> in synchronous fluorescence spectroscopy, the difference between the excitation and emission wavelength ( $\Delta\lambda = \lambda_{emi} - \lambda_{exc}$ ) reflects the spectra of a different nature of chromophores with small  $\Delta\lambda$  value such as 15 nm is the characteristic of tyrosine residue and the large  $\Delta\lambda$  value such as 60 nm is the characteristic of tryptophan residue. In order to study the structural changes of BSA in the presence of nickel(II) hydrazone complexes, we measured synchronous fluorescence spectra with the addition of complexes 1-4.

The synchronous fluorescence spectra of BSA with nickel(II) hydrazone complexes 1-4 were recorded at both  $\Delta\lambda = 15$  nm and  $\Delta\lambda = 60$  nm are shown in Fig. 11 and 12. In the synchronous fluorescence spectra of BSA at  $\Delta\lambda = 15$  nm, increasing the concentration of complexes to the solution of BSA resulted in decrease of fluorescence intensity of BSA at 302 nm, 30.84%, 32.78%, 33.18% and 34.71% 1-2 nm red shift of the initial fluorescence intensity of BSA for complexes 1-4 respectively. However, in the case of the synchronous fluorescence spectra of BSA at  $\Delta\lambda = 60$  nm, an increase in the

concentration of the complexes to the solution of BSA resulted in a significant decrease of the fluorescence intensity at 345 nm, up to 51.40%, 37.71%, 34.20% and 51.75% of the initial fluorescence intensity of BSA accompanied by 1-2 nm blue shift for complexes 1-4.

These experimental results indicate that nickel(II) benzhydrazone complexes does not affect the with residues led to a decrease in the polarity of the fluorophore by an increasing the hydrophobicity around the same. Hence, the strong interaction between the complexes with BSA demonstrates that these complexes can easily stored in protein and can be released in desired targets. The characretics of the synchronous fluorescence measurements show the conformational changes occurred in BSA upon interaction with nickel(II) benzhydrazone complexes.

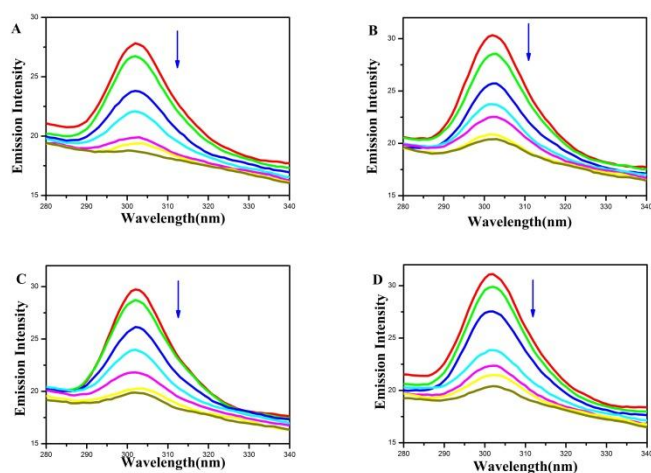


**Fig. 11** The Synchronous fluorescence spectra of BSA(1 $\mu$ M) as a function of concentration of complexes 1(A), 2(B), 3(C), and 4(D)(0-60 $\mu$ M) with a wave length difference of  $\Delta\lambda=15$ nm.

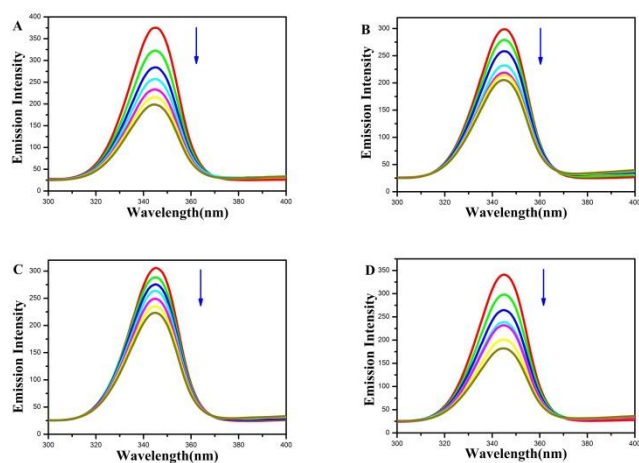


**Fig. 12** The Synchronous fluorescence spectra of BSA(1 $\mu$ M) as a function of concentration of complexes 1(A), 2(B), 3(C), and 4(D)(0-60 $\mu$ M) with a wave length difference of  $\Delta\lambda=60$  nm.

### BSA cleavage studies

When the ability of the complexes to cleave protein peptide bonds<sup>72</sup> was studied using BSA as substrate. The experiment

was carried out using BSA (20  $\mu$ M) in 5 mM Tris-HCl-50 mM NaCl buffer at  $p^H = 7.2$ . In the absence of an activator like hydrogen peroxide, all the complexes does not show any protein cleavage even at 500  $\mu$ M concentration of complexes. When the cleavage experiment was done at 200  $\mu$ M complex in the presence of  $H_2O_2$  (100  $\mu$ M) at  $p^H 7.2$  (Fig. 13) all the complexes show significant smearing or fading of the BSA band suggesting that the complexes bind non-specifically to the protein and cleave BSA into very small fragments. All the complexes are capable of cleaving the protein, but without any sequence specificity.

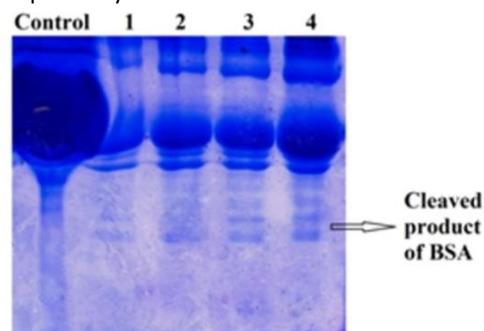


**Fig.13** SDS-PAGE diagram of the cleavage of bovine serum albumin BSA by complexes 1-4 [BSA]= 20  $\mu$ M [complexes]=200  $\mu$ M in 5 mM Tris-HCl-50 mM NaCl buffer at  $p^H = 7.2$  and in the presence of hydrogen peroxide ( $H_2O_2$ , 100  $\mu$ M) at 50  $^{\circ}C$  with an incubation time of 3 h. Lane 1, BSA +  $H_2O_2$ ; lane 2, BSA +  $H_2O_2$  + 1; lane 3, BSA +  $H_2O_2$  + 2; lane 4, BSA +  $H_2O_2$  + 3; lane 5, BSA +  $H_2O_2$  + 4.

### Antioxidant activity

In order to evaluate the ability of the nickel(II) benzhydrazone complexes to act toward different reactive species, we studied some radical scavenging assay methods, in particular DPPH, OH and NO radicals scavenging assays (Fig 14). The hydrazone ligands, metallic precursors and nickel(II) benzhydrazone complexes have been tested in the range of 10-50  $\mu$ M. It is to be noted that no significant radical scavenging activities were observed for ligands and the metallic precursors under the identical experimental conditions. From the experimental results the  $IC_{50}$  value of the complexes with respect to DPPH, OH and NO radicals assays were found to be 41.6, 40, 40.8, 34.5  $\mu$ M, 41.6, 40.81, 40, 35.0  $\mu$ M, 44.1, 43, 41.8 and 38.1  $\mu$ M respectively. The  $IC_{50}$  values show that the complexes exhibit antioxidant activity in the order of 4 > 2 > 3 > 1 > ligand > precursors in all of the experiments. The complexes 1-4 displayed almost comparable free radical scavenging activity with respect to the standard antioxidant (BHA). From the  $IC_{50}$ , it can be concluded that the nickel complexes having higher antioxidant activity when compared to free ligand and metallic precursors, which is due to the chelation of them with the metal ions. Among the complexes, complex 4 shows good radical scavenging activity and this might be due to the more electron donating nature of the methoxy substituent and the planarity of the phenyl group. The lowest activity was observed for complex 1. Hence, we strongly consider that the present metal hydrazone complexes can be further evaluated as suitable candidates leading to the development of new potential antioxidants and therapeutic reagents for some diseases.

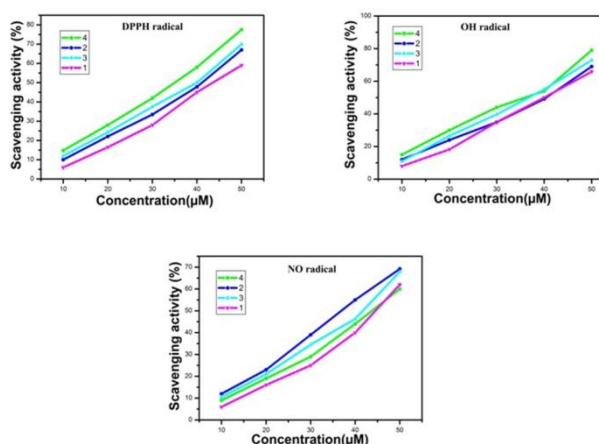


Fig. 14 Trends in the inhibition of DPPH, OH and NO radicals by complexes at various concentrations.

### Cytotoxicity

Preliminary up-to-date results are remarkably positive, thus supporting our facts and confirming the tremendous potential of this class of nickel complexes as anticancer agents.<sup>73</sup> Nickel hydrazone complexes 1-4 were evaluated for their cytotoxicity against HeLa, MCF-7 and NIH-3T3 cell lines using MTT assay after 48 hours of inhibition. For comparison, the cytotoxicity of the well known anti-cancer drug cisplatin against all the above cell lines are shown in Table 5. The results were studied by means of cell viability curves and expressed with values in the studied concentration range from 0.1-100  $\mu\text{M}$ . The activity corresponding to inhibition of cancer cell growth at maximum level as expressed as  $\text{IC}_{50}$  values were related to inhibition of cancer cell growth at the 50% level, are noted.

Table 5 The cytotoxic activity of the complexes. <sup>a</sup>  $\text{IC}_{50}$  ( $\mu\text{M}$ )

Complex	HeLa	MCF-7	NIH-3T3
1	52.3 $\pm$ 1.5	22.4 $\pm$ 2.1	235.60 $\pm$ 0.5
2	32.1 $\pm$ 1.8	18.2 $\pm$ 1.1	238.72 $\pm$ 1.4
3	37.1 $\pm$ 2.1	17.8 $\pm$ 1.9	242.32 $\pm$ 2.0
4	18.1 $\pm$ 1.9	16.3 $\pm$ 0.9	245.64 $\pm$ 1.1
Cisplatin	16.20 $\pm$ 0.70	13.86 $\pm$ 0.5	240.52 $\pm$ 0.6

<sup>a</sup>  $\text{IC}_{50}$  = Concentration of the drug required to inhibit growth of 50% of the cancer cells ( $\mu\text{M}$ )

It is to be esteemed that the precursor and the ligand did not display any inhibition of the cell growth even up to 100  $\mu\text{M}$  and clearly indicates chelation of the ligand with metal ion is responsible for the observed cytotoxicity properties of the complexes. The results of MTT assays revealed that complexes showed notable activity against both the cell lines HeLa and MCF-7 with respect to  $\text{IC}_{50}$  values is represented in Table 5. The cytotoxic activity of the complex 4 is found to be very superior when compared to other complexes. The observed higher efficiency of the complex 4 is correlated to the nature of the substitution of the benzhydrazone ligand coordinated to

the nickel ion in it. The higher cytotoxicity is observed for complex 4 which containing electron donating methoxy group subsequently increases the lipophilic character of the metal complex which favours its permeation through the lipid layer of the cell membrane. Among the two different cell lines used in that is study, the proliferation of MCF-7 cell lines was arrested to a greater extent than HeLa cells by the complexes. Though the above mentioned complexes are active against the cell lines under in vitro cytotoxicity experiments, none of the complexes could reach the effectiveness shown by the standard drug cisplatin ( $\text{IC}_{50}$  value 16.20 and 13.86  $\mu\text{M}$ , respectively). The in vitro cytotoxic activity have also shows that the  $\text{IC}_{50}$  value of complex against NIH-3T3 (non-cancerous cells) is found to be above 235  $\mu\text{M}$ , which confirmed that the complex is very specific for cancer cells compared to cisplatin. The  $\text{IC}_{50}$  values are much better than those previously reported for the other nickel complexes.<sup>74</sup>

### Neutral Red Uptake Assay

The  $\text{IC}_{50}$  values obtained from MTT assay were further evaluated by the neutral red uptake assay by taking HeLa cell lines. The neutral red uptake assay provides a quantitative estimation of the number of viable cells in a culture. It is based on the ability of viable cells to incorporate and bind the supravital dye neutral red in the lysosomes. Dying cells have altered membrane potential and therefore they cannot anymore take up neutral red. The dye is applied to cells in different concentrations allowing the determination of  $\text{IC}_{50}$  concentration (50% reduction of uptake) by measuring  $\text{OD}_{540}$ .

The HeLa cells were exposed to different concentrations of the nickel(II) benzhydrazone complexes 1-4 for 48 h incubation. The results of  $\text{IC}_{50}$  value shows 50.0  $\pm$  1.2, 33.2  $\pm$  1.0, 36.5  $\pm$  0.9 and 20.1  $\pm$  1.0 for the complexes 1-4 respectively and these values are found to be very close to the values obtained from MTT assay.

### Morphological changes in AO and EB dual staining by confocal study

Upon exposure to cytotoxic agents the cell death may take place by several modes and among these apoptosis and necrosis are very common. Apoptosis or programmed cell death is characterized by cell shrinkage, blebbing of the plasma membrane, and chromatin condensation. To investigate the morphological changes Acridine Orange and Ethidium Bromide (AO and EB) dual staining technique is frequently used. In order to investigate the mechanistic aspects of cell death and to determine the changes of nuclear morphology, AO and EB dual staining of the MCF-7 cell lines treated with complex 4 (10  $\mu\text{M}$ ) was carried out and shown in (Fig.15). The experiment was based on the discrimination of live cells from the dead cells on the basis of morphological changes. Acridine orange passes through the plasma membrane and stains the DNA of live cells with the appearance of green fluorescence. On the other hand, EB is excluded from the cells having intact plasma membrane and stains the DNA of dead cells, showing orange fluorescence. The cells incubated with the complex 4 for 24 h and irradiated with

visible light showed significant reddish–orange emission characteristic of the apoptotic cells. The controls, which were incubated in dark, showed only predominant green emission. Hence, the observed morphological changes reveal that the complex 4 is able to induce cell death only through apoptosis.

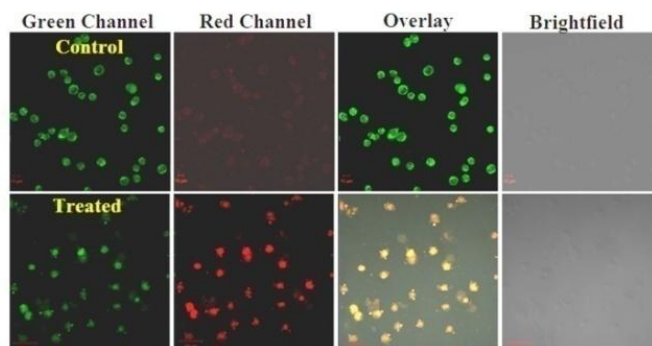


**Fig.15** AO and EB dual staining of MCF-7 cells treated with complex 4 (10  $\mu$ M) showing the changes in nuclear morphology at 488–600 nm. The scale bar corresponds to 50  $\mu$ m.

#### Nuclear DAPI staining experiment by confocal study

To further confirm the apoptosis mode, DAPI staining was also carried out. DAPI is a fluorescent nuclear stain, excited by ultraviolet light and showing strong blue fluorescence when bound to DNA. The control and complex 4 (100  $\mu$ g mL<sup>-1</sup>) treated cells were stained with DAPI and observed under confocal microscope (Fig.16). The control cells permeabilized with detergent (0.1% Triton X-100) exhibit light and evenly stained contours of the nuclei in contrast to the treated cells that show typical characteristics of cells undergoing apoptosis. The treated cells are seen to possess fragmented or highly condensed nuclei while the bright field images provide evidence for cell shrinkage and membrane blebbing attributed to the typical features of apoptotic cells. Necrotic nuclei are not observed with DAPI staining. Hence the DAPI staining indicates apoptotic mode of cell death with the complex.

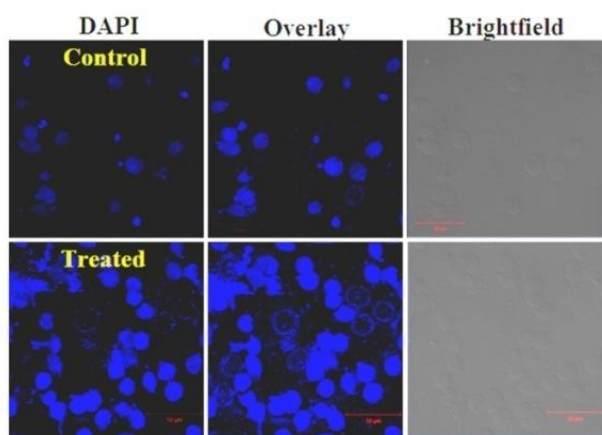


**Fig.16** Morphological assessment of complex 4 and MCF-7 cells for 24 h. Nuclei were stained with DAPI and observed under confocal microscope of 458 nm.

#### Evaluation of Apoptosis - Flow Cytometry

The ability to induce apoptosis by nickel(II) benzhydrazone complex was further investigated with the aid of flow cytometry, using the Annexin V-FITC Apoptosis Detection Kit to perform double-staining with propidium iodide and Annexin V-FITC.<sup>51</sup> Annexin V, a Ca<sup>2+</sup> dependent phospholipid-binding protein with a high affinity for the membrane phospholipid phosphatidylserine (PS), is quite helpful for identifying apoptotic cells with exposed PS. Propidium iodide is a standard flow cytometric viability probe used to distinguish viable from non-viable cells. The MCF-7 cells were treated with the complex 4 at three different concentrations for 48 h. Fig.17. Annexin V<sup>+</sup>/PI<sup>+</sup> (Q<sub>2</sub>) population represented cells undergoing apoptosis with increasing from 30.7%, 48.6% and 52.7% for 50  $\mu$ M, 100  $\mu$ M and 200  $\mu$ M concentrations of the complexes. This observation is in good agreement with the results obtained from fluorescence staining methods.

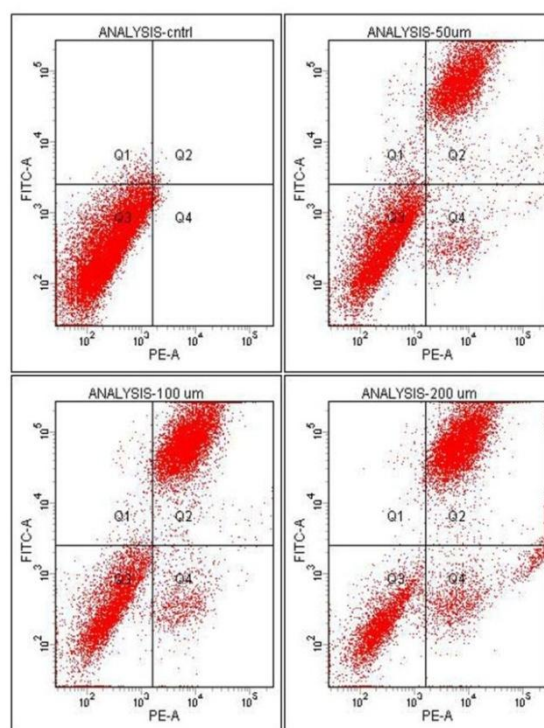


**Fig.17** Apoptosis Assays: Propidium iodide and annexin positive (Q<sub>2</sub>) and propidium iodide positive (Q<sub>4</sub>); Flow cytometry results of untreated MCF-7 control cells and cells treated with complex-4 at 50 $\mu$ M, 100 $\mu$ M and 200 $\mu$ M concentration for 48h respectively.

#### Conclusion

The present work focuses on the synthesis and characterization of four new square planar nickel(II) complexes with thiophene aldehyde benzhydrazone ligands. The characterizations of the complexes were accomplished by analytical and spectral methods. All the complexes were found to have a metal to ligand molar ratio of 1:2 composition. All the complexes show one electron quasi-reversible reduction response versus SCE. The DNA binding interactions of the

complexes with CT-DNA shows that the binding mode is essentially non-covalent via intercalation. The binding constants showed that the DNA binding ability increased in the order of  $4 > 2 > 3 > 1$ . Competitive binding studies with EB revealed that the ability of the complexes to displace EB from the EB-DNA complex. The cyclic voltammetric and viscosity measurements confirm the intercalation mode of binding of the nickel(II) complex to CT-DNA. The CD spectral results lead to no conformational change of DNA is observed. The interactions between nickel(II) benzhydrazone complexes and BSA in buffer solution studied by UV-Vis, fluorescence and synchronous fluorescence methods did suggest that the complexes possess strong binding ability to quench the BSA fluorescence mainly through a static quenching mechanism. The results of synchronous fluorescence measurements revealed that the present complexes did influence the micro-environment around both tyrosine and tryptophan residues of BSA. The binding constants showed that the protein binding ability increased in the order of  $4 > 2 > 3 > 1$ . The antioxidant results indicated that all the complexes have almost comparable values against BHA. In addition, all the complexes showed significant cytotoxicity against HeLa and MCF-7 cell lines without affecting the normal NIH-3T3 cell much. Further the fluorescence staining techniques and flow cytometry using Annexin-V assay revealed that the complex 4 induces apoptosis in cancer cells.

## Acknowledgements

R.R.K thank to DST-INSPIRE Program for the financial assistant as a JRF (IF130075). We thank UGC-SAP and DST-India (FIST programme) for the use of Bruker 400 MHz NMR, UV-Visible and fluorescence spectral facilities at the School of chemistry, Bharathidasan University. We thank Prof. A. Ramu, Madurai Kamaraj University and Prof. N. Thajuddin, Bharathidasan University, for providing the CD and confocal instrumental facilities. We thank to Dr. Sanjib karmakar, SAIF, Department of Instrumentation & USIC, Gauhati University, Guwahati for collecting single crystal X-ray diffraction data. We also thank the CSIR, New Delhi for electrochemical analyser through research project [Ref. No: 02(0142)/13/EMR-II].

## References

1. S. Leininger, B. Olenyuk and P. J. Stang, *Chemical Reviews*, 2000, **100**, 853-908.
2. S. Feng and R. Xu, *Acc Chem Res*, 2001, **34**, 239-247.
3. B. Spingler, C. Da Pieve, A. Medina-Molner, P. M. Antoni and M. G. Santangelo, *CHIMIA International Journal for Chemistry*, 2009, **63**, 153-156.
4. G. Zuber, J. C. Quada and S. M. Hecht, *Journal of the American Chemical Society*, 1998, **120**, 9368-9369.
5. B. Rosenberg, L. VanCamp, J. E. Trosko and V. H. Mansour, *Nature*, 1969, **222**, 385-386.
6. B. Rosenberg, L. Van Camp and T. Krigas, *Nature*, 1965, **205**, 698-699.
7. J. M. Rademaker-Lakhai, D. van den Bongard, D. Pluim, J. H. Beijnen and J. H. Schellens, *Clin Cancer Res*, 2004, **10**, 3717-3727.
8. M. A. Jakupec and B. K. Keppler, *Current Topics in Medicinal Chemistry*, 2004, **4**, 1575-1583.
9. P. J. Barnard and S. J. Berners-Price, *Coordination Chemistry Reviews*, 2007, **251**, 1889-1902.
10. B. P. Espósito and R. Najjar, *Coordination Chemistry Reviews*, 2002, **232**, 137-149.
11. J. E. Patterson and D. M. Geller, *Biochemical and Biophysical Research Communications*, 1977, **74**, 1220-1226.
12. R. T. A. MacGillivray, D. W. Chung and E. W. Davie, *European Journal of Biochemistry*, 1979, **98**, 477-485.
13. K. Hirayama, S. Akashi, M. Furuya and K. Fukuhara, *Biochem Biophys Res Commun*, 1990, **173**, 639-646.
14. U. Kragh-Hansen, *Pharmacol Rev*, 1981, **33**, 17-53.
15. I. Cantuti-Castelvetri, B. Shukitt-Hale and J. A. Joseph, *International Journal of Developmental Neuroscience*, 2000, **18**, 367-381.
16. Y.-J. Surh, K.-S. Chun, H.-H. Cha, S. S. Han, Y.-S. Keum, K.-K. Park and S. S. Lee, *Mutation Research/Fundamental and Molecular Mechanisms of Mutagenesis*, 2001, **480-481**, 243-268.
17. J. Vaya and M. Aviram, *Current Medicinal Chemistry - Immunology, Endocrine & Metabolic Agents*, 2001, **1**, 99-117.
18. O. I. Aruoma, *Mutation Research/Fundamental and Molecular Mechanisms of Mutagenesis*, 2003, **523-524**, 9-20.
19. K. J. A. Davies, *IUBMB Life*, 2000, **50**, 279-289.
20. A. C. Torbergesen and A. R. Collins, *Eur J Nutr*, 2000, **39**, 80-85.
21. P. K. Singh and D. N. Kumar, *Spectrochimica Acta Part A: Molecular and Biomolecular Spectroscopy*, 2006, **64**, 853-858.
22. B. Singh, R. Srivastava and K. K. Narang, *Synthesis and Reactivity in Inorganic and Metal-Organic Chemistry*, 2000, **30**, 1175-1192.
23. J. D. Ranford, J. J. Vittal and Y. M. Wang, *Inorganic Chemistry*, 1998, **37**, 1226-1231.
24. J. L. Buss, B. T. Greene, J. Turner, F. M. Torti and S. V. Torti, *Curr Top Med Chem*, 2004, **4**, 1623-1635.
25. P. S. Donnelly, A. Caragounis, T. Du, K. M. Laughton, I. Volitakis, R. A. Cherny, R. A. Sharples, A. F. Hill, Q. X. Li, C. L. Masters, K. J. Barnham and A. R. White, *J Biol Chem*, 2008, **283**, 4568-4577.
26. V. Martin-Diaconescu and M. J. Maroney, in *Comprehensive Inorganic Chemistry II (Second Edition)*, ed. J. R. Poeppelemeier, Elsevier, Amsterdam, 2013, DOI:<http://dx.doi.org/10.1016/B978-0-08-097774-4.00319-3>, pp. 295-322.
27. L. Signor, C. Knuppe, R. Hug, B. Schweizer, A. Pfaltz and B. Jaun, *Chemistry – A European Journal*, 2000, **6**, 3508-3516.

28. C. J. Campbell, J. F. Rusling and C. Brückner, *Journal of the American Chemical Society*, 2000, **122**, 6679-6685.
29. M. P. Sathisha, U. N. Shetti, V. K. Revankar and K. S. R. Pai, *European Journal of Medicinal Chemistry*, 2008, **43**, 2338-2346.
30. S. M. Pradeepa, H. S. Bhojya Naik, B. Vinay Kumar, K. Indira Priyadarsini, A. Barik and T. R. Ravikumar Naik, *Spectrochimica Acta Part A: Molecular and Biomolecular Spectroscopy*, 2013, **101**, 132-139.
31. S.-Y. Lee, A. Hille, C. Frias, B. Kater, B. Bonitzki, S. Wöfl, H. Scheffler, A. Prokop and R. Gust, *Journal of Medicinal Chemistry*, 2010, **53**, 6064-6070.
32. H. Wu, J. Yuan, Y. Bai, G. Pan, H. Wang and X. Shu, *Journal of Photochemistry and Photobiology B: Biology*, 2012, **107**, 65-72.
33. E. Ramachandran, D. Senthil Raja, N. S. P. Bhuvanesh and K. Natarajan, *European Journal of Medicinal Chemistry*, 2013, **64**, 179-189.
34. X. Totta, A. A. Papadopoulou, A. G. Hatzidimitriou, A. Papadopoulos and G. Psomas, *Journal of Inorganic Biochemistry*, 2015, **145**, 79-93.
35. P. Krishnamoorthy, P. Sathyadevi, R. R. Butorac, A. H. Cowley, N. S. P. Bhuvanesh and N. Dharmaraj, *Dalton Transactions*, 2012, **41**, 6842-6854.
36. A. R. B. Rao and S. Pal, *Journal of Organometallic Chemistry*, 2011, **696**, 2660-2664.
37. S. Anbu, M. Kandaswamy and B. Varghese, *Dalton Transactions*, 2010, **39**, 3823-3832.
38. I. M. SADABS: Area- Detector Absorption Correction; Siemens Industrial Automation, WI, 1996.
39. G. Sheldrick, *Acta Crystallographica Section A*, 2008, **64**, 112-122.
40. W. Bruker-Nonious (2004) and M. Bruker Axs Inc., USA.
41. P. Lincoln, E. Tuite and B. Nordén, *Journal of the American Chemical Society*, 1997, **119**, 1454-1455.
42. B. Nordén and F. Tjerneld, *Biopolymers*, 1982, **21**, 1713-1734.
43. J. B. Chaires, N. Dattagupta and D. M. Crothers, *Biochemistry*, 1982, **21**, 3933-3940.
44. G. Cohen and H. Eisenberg, *Biopolymers*, 1969, **8**, 45-55.
45. C. V. Kumar, A. Buranaprapuk, H. C. Sze, S. Jockusch and N. J. Turro, *Proceedings of the National Academy of Sciences*, 2002, **99**, 5810-5815.
46. M. S. Blois, *Nature*, 1958, **181**, 1199-1200.
47. T. Nash, *Biochemical Journal*, 1953, **55**, 416-421.
48. L. C. Green, D. A. Wagner, J. Glogowski, P. L. Skipper, J. S. Wishnok and S. R. Tannenbaum, *Analytical Biochemistry*, 1982, **126**, 131-138.
49. T. Mosmann, *Journal of Immunological Methods*, 1983, **65**, 55-63.
50. G. Repetto, A. del Peso and J. L. Zurita, *Nat. Protocols*, 2008, **3**, 1125-1131.
51. I. Vermes, C. Haanen, H. Steffens-Nakken and C. Reutellingsperger, *Journal of Immunological Methods*, 1995, **184**, 39-51.
52. L. J. Ackerman, P. E. Fanwick, M. A. Green, E. John, W. E. Running, J. K. Swearingen, J. W. Webb and D. X. West, *Polyhedron*, 1999, **18**, 2759-2767.
53. R. Raveendran and S. Pal, *Journal of Organometallic Chemistry*, 2007, **692**, 824-830.
54. M. Sönmez, A. Levent and M. Şekerci, *Russian Journal of Coordination Chemistry*, 2004, **30**, 655-660.
55. N. Selvakumaran, A. Pratheepkumar, S. W. Ng, E. R. T. Tiekink and R. Karvembu, *Inorganica Chimica Acta*, 2013, **404**, 82-87.
56. K. Mitra, S. Biswas, C. R. Lucas and B. Adhikary, *Inorganica Chimica Acta*, 2006, **359**, 1997-2003.
57. Y. Kurt, A. Koca, M. Akkurt and B. Ülküseven, *Inorganica Chimica Acta*, 2012, **388**, 148-156.
58. S. V. Kryatov, B. S. Mohanraj, V. V. Tarasov, O. P. Kryatova, E. V. Rybak-Akimova, B. Nuthakki, J. F. Rusling, R. J. Staples and A. Y. Nazarenko, *Inorganic Chemistry*, 2002, **41**, 923-930.
59. C. Hansch, A. Leo and R. W. Taft, *Chemical Reviews*, 1991, **91**, 165-195.
60. D. Senthil Raja, N. S. P. Bhuvanesh and K. Natarajan, *Inorganic Chemistry*, 2011, **50**, 12852-12866.
61. V. Uma, M. Kanthimathi, T. Weyhermuller and B. U. Nair, *Journal of Inorganic Biochemistry*, 2005, **99**, 2299-2307.
62. X.-L. Wang, H. Chao, H. Li, X.-L. Hong, Y.-J. Liu, L.-F. Tan and L.-N. Ji, *Journal of Inorganic Biochemistry*, 2004, **98**, 1143-1150.
63. C. Tan, J. Liu, L. Chen, S. Shi and L. Ji, *Journal of Inorganic Biochemistry*, 2008, **102**, 1644-1653.
64. M. T. Carter, M. Rodriguez and A. J. Bard, *Journal of the American Chemical Society*, 1989, **111**, 8901-8911.
65. S.-S. Zhang, S.-Y. Niu, B. Qu, G.-F. Jie, H. Xu and C.-F. Ding, *Journal of Inorganic Biochemistry*, 2005, **99**, 2340-2347.
66. Y. Ni, D. Lin and S. Kokot, *Analytical Biochemistry*, 2006, **352**, 231-242.
67. H. Liu, L. Li, Q. Guo, J. Dong and J. Li, *Transition Metal Chemistry*, 2013, **38**, 441-448.
68. S. Satyanarayana, J. C. Dabrowiak and J. B. Chaires, *Biochemistry*, 1992, **31**, 9319-9324.
69. S. Satyanarayana, J. C. Dabrowiak and J. B. Chaires, *Biochemistry*, 1993, **32**, 2573-2584.
70. X. Z. H. G.Z.Zen, J.G.Xu,Z.Z.Zheng and Z.B.Wang, *Methods of Fluorescence Analysis*, Science press, Beijing, 2 edn., 1990.
71. C. W. Fuller and J. N. Miller, *Proceedings of the Analytical Division of the Chemical Society*, 1979, **16**, 199-208.
72. T. N. Parac and N. M. Kostić, *Journal of the American Chemical Society*, 1996, **118**, 51-58.
73. Z. Afrasiabi, E. Sinn, S. Padhye, S. Dutta, S. Padhye, C. Newton, C. E. Anson and A. K. Powell, *Journal of Inorganic Biochemistry*, 2003, **95**, 306-314.
74. P. Sathyadevi, P. Krishnamoorthy, R. R. Butorac, A. H. Cowley, N. S. P. Bhuvanesh and N. Dharmaraj, *Dalton Transactions*, 2011, **40**, 9690-9702.



28x25mm (150 x 150 DPI)